Journal of Computational Physics 446 (2021) 110627

Contents lists available at ScienceDirect

Journal of Computational Physics

www.elsevier.com/locate/jcp

A frequency-dependent p-adaptive technique for spectral methods

Mingtao Xia[a], Sihong Shao[b,*], Tom Chou[a,*]

[a] Department of Mathematics, UCLA, Los Angeles, CA 90095-1555, USA
[b] LMAM and School of Mathematical Sciences, Peking University, Beijing 100871, China

ARTICLE INFO

Article history:
Available online 17 August 2021

Keywords:
Adaptive spectral method
Schrödinger equation
Unbounded domains
Jacobi polynomial
Hermite function
Laguerre function

ABSTRACT

When using spectral methods, a consistent method for tuning the expansion order is often required, especially for time-dependent problems in which oscillations emerge in the solution. In this paper, we propose a frequency-dependent p-adaptive technique that adaptively adjusts the expansion order based on a frequency indicator. Using this p-adaptive technique, combined with recently proposed scaling and moving techniques, we are able to devise an adaptive spectral method in unbounded domains that can capture and handle diffusion, advection, and oscillations. As an application, we use this adaptive spectral method to numerically solve Schrödinger's equation in an unbounded domain and successfully capture the solution's oscillatory behavior at infinity.

1. Introduction

Unbounded domain problems arise in many scientific applications [1,2] and adaptive numerical methods are needed on many occasions, for instance, in solving Schrödinger's equation in unbounded domains when the solution varies rapidly in time. As an important class of numerical algorithms, adaptive methods have witnessed numerous advances in their efficiency and accuracy [3–6]. However, despite considerable progress that has been made for spectral methods in unbounded domains [7], there are few adaptive methods that apply in unbounded domains.

In [8], adaptive scaling and moving techniques were proposed for spectral methods in unbounded domains and it was noted that adjusting the expansion order is necessary when the function displays oscillatory behavior that varies over time. In this paper, we first develop a frequency-dependent technique for spectral methods which adjusts the expansion order N ($N+1$ basis functions are used to approximate the solution). This technique takes advantage of the frequency indicator defined in [8] and corresponds to p-adaptivity [9–11,21,22]. By adjusting the expansion order efficiently, our p-adaptive technique can be used to accurately solve problems with varying oscillatory behavior.

Although the work reported in [8] motivated us to develop a complementary p-adaptive technique using the same frequency indicator for the numerical solutions, the expansion order in [8] remained fixed, while in this work it is adaptively adjusted according to the dynamic behavior of the unknown functions. For instance, as demonstrated in Examples 6 and 7 and in the subsequent discussion, solutions to Schrödinger's equation that become increasingly oscillatory over time cannot be well approximated by the previously proposed scaling and moving techniques [8]. On the other hand, a p-adaptive technique that only adjusts the expansion cannot successfully deal with diffusing and advecting solutions, which

[*] Corresponding authors.
E-mail addresses: xiamingtao97@g.ucla.edu (M. Xia), sihong@math.pku.edu.cn (S. Shao), tomchou@ucla.edu (T. Chou).

https://doi.org/10.1016/j.jcp.2021.110627

are captured by the moving and scaling techniques described in [8], as shown in Examples 4, 5, and 8. Thus, an efficient and more complete adaptive spectral method should integrate moving, scaling, and p-adaptive techniques as outlined in Fig. 5.

By combining this p-adaptive technique with scaling and moving methods, we develop an adaptive spectral method that can capture diffusion, advection, and oscillations in unbounded domains. Since scaling and adjusting the expansion order both depend on the frequency indicator, we also investigate the interdependence of these two techniques. We demonstrate that appropriately adjusting the expansion order can facilitate scaling to more efficiently distribute allocation points. In turn, proper scaling can help avoid unnecessary increases in the expansion order when it does not increase accuracy, thereby avoiding unnecessary computational burden.

The significance of this adaptive spectral method is that it can capture the solution's behavior in the whole domain $\mathbb{R}$. We demonstrate the utility of our method by solving Schrödinger's equation in $\mathbb{R}$. Here, the unboundedness and the oscillatory nature of the solution pose two major numerical challenges [12]. Specifically, in the semiclassical regime, when the wavelength of the solution is small, the function becomes extremely oscillatory. Moreover, in certain situations, one has to work with a very large computational domain that is difficult to automatically determine.

Previous numerical methods which solve Schrödinger's equation in unbounded domains usually truncate the domain into a finite subdomain and impose artificial boundary conditions, which may be nonlocal and complicated [12–15]. Our adaptive spectral method tackles the oscillatory problem directly in the original unbounded domain without the need to truncate it or to devise an artificial boundary condition.

In the next section, we first present a p-adaptive technique for spectral methods and use examples to illustrate its efficiency. In Section 3, we incorporate and study this technique within existing scaling and moving techniques and devise an adaptive spectral method in unbounded domains. Application of our adaptive spectral methods to numerically solving Schrödinger's equation is given in Section 4. We summarize our results in Section 5 and propose directions for future work.

2. Frequency-dependent p-adaptivity

We present a frequency-dependent p-adaptive spectral method based on information extracted from only the numerical solution of time-dependent problems. In [8], we showed that a frequency indicator defined for spectral methods is particularly useful in measuring the contribution of high frequency modes in the numerical solution. Because high frequency modes decay more slowly, this indicator could be used to determine scaling in spectral methods applied to unbounded domains.

In this work, we will show that the frequency indicator can also be used to determine whether more or fewer basis functions are needed to refine or coarsen the numerical solution. Proper refining allows one to maintain accuracy when the solution becomes more oscillatory, while appropriate coarsening reduces computational costs without sacrificing accuracy.

Given a set of orthogonal basis functions $\{B_i(x)\}_{i=0}^{\infty}$ under a specific weight function $\omega(x) > 0$ in a domain Λ, the frequency indicator associated with the interpolation of a function

$$\mathcal{I}_N u(x) = U_N(x) = \sum_{i=0}^{N} u_i B_i(x) \tag{2.1}$$

is defined as in [8]

$$\mathcal{F}(U_N) := \left(\frac{\sum\limits_{i=N-M+1}^{N} \gamma_i u_i^2}{\sum\limits_{i=0}^{N} \gamma_i u_i^2} \right)^{\frac{1}{2}}, \tag{2.2}$$

where $\gamma_i = \int_\Lambda B_i^2(x)\omega(x)\mathrm{d}x$ is the square of L^2_ω-weighted norm of the basis function $B_i(x)$. This frequency indicator measures the contribution of the M highest-frequency components to the L^2_ω-weighted norm of U_N. Here M is often chosen to be $[\frac{N}{3}]$ following the $\frac{2}{3}$-rule [16,17]. This indicator provides a lower bound for the error divided by the norm of the numerical solution $\frac{\|u-\mathcal{I}_{N-M}u\|_\omega}{\|\mathcal{I}_N u\|_\omega}$ which is illustrated in [8]. Thus, the quality of the numerical interpolation U_N can be measured by $\mathcal{F}(U_N)$.

For a time-dependent problem, the expansion order N may need adjusting dynamically, which can be reflected by the frequency indicator. If the frequency indicator increases, the lower bound for $\frac{\|u-\mathcal{I}_{N-M}u\|_\omega}{\|\mathcal{I}_N u\|_\omega}$ will also increase. On the other hand, as N increases, the error $\|u - \mathcal{I}_N u\|_\omega$ as well as $\mathcal{F}(U_N)$ are expected to decrease. By sufficiently increasing the expansion order N, the frequency indicator as well as the error can be kept small. If the frequency indicator decreases, we can also consider decreasing N to relieve computational costs without compromising accuracy, as was done in [9]. The pseudo-code of the proposed p-adaptive technique is given in Algorithm 1.

The p-adaptive spectral method in Algorithm 1 for time-dependent problems consists of two ingredients: refinement (increasing N) and coarsening (decreasing N). The method maintains accuracy when there are emerging oscillations by increasing the expansion order N. It also decreases N when the expansion order is larger than needed to avoid unnecessary

Algorithm 1 Pseudo-code of the p-adaptive technique which may increase (refine) or decrease (coarsen) the expansion order N.

```
1: Initialize $N, N_0, \gamma \geq 1, \eta_0 = \eta > 1, \Delta t, T, \alpha, \beta, U_N(0), N_{\max}, N_{\min}$
2: $t \leftarrow 0$
3: $f_0 \leftarrow$ FREQUENCY_INDICATOR($U_N(t)$)
4: while $t < T$ do
5:     $U_N(t+\Delta t) \leftarrow$ EVOLVE($U_N(t), \Delta t$)
6:     $f \leftarrow$ FREQUENCY_INDICATOR($U_N(t+\Delta t)$)
7:     $l \leftarrow 0$
8:     if $f > \eta f_0$ then    # refinement is needed
9:         while $f > \eta f_0$ and $l \leq N_{\max}$ do
10:            $l \leftarrow l+1$
11:            $U_{N+1} \leftarrow$ REFINE($U_N(t+\Delta t)$)
12:            $N \leftarrow N+1$
13:            $f \leftarrow$ FREQUENCY_INDICATOR($U_N$)
14:        end while
15:        $f_0 \leftarrow f$
16:        $\eta \leftarrow \gamma\eta$    # renew $\eta$
17:    else if $f < f_0/\eta_0$ then    # coarsening could be considered
18:        $r \leftarrow$ False
19:        while $f < f_0/\eta_0$ and $N > N_{\min}$ do
20:            $\tilde{U}_{N-1}(t+\Delta t) \leftarrow$ COARSEN($U_N(t+\Delta t)$)
21:            $f \leftarrow$ FREQUENCY_INDICATOR($\tilde{U}_{N-1}(t+\Delta t)$)
22:            if $f < f_0$ then
23:                $f_1 \leftarrow f$
24:                $r \leftarrow$ True
25:                $U_{N-1}(t+\Delta t) \leftarrow \tilde{U}_{N-1}(t+\Delta t)$
26:                $N \leftarrow N-1$
27:            end if
28:        end while
29:        if $r$ then
30:            $f_0 \leftarrow f_1$
31:        end if
32:    end if
33:    $t \leftarrow t+\Delta t$
34: end while
```

computation. In Algorithm 1, the FREQUENCY_INDICATOR subroutine evaluates the frequency indicator defined in Eq. (2.2) for the numerical solution U_N while the EVOLVE subroutine is to obtain the numerical solution $U_N(t+\Delta t)$ at the next timestep from $U_N(t)$.

In Line 11 of Algorithm 1, the REFINE subroutine uses U_N to generate a new numerical solution with a larger expansion order U_{N+1} (refine), and in Line 20 the COARSEN subroutine uses U_N to generate a new numerical solution with a smaller expansion order U_{N-1} (coarsen). The refinement or coarsening is achieved by reconstructing the function values of U_{N+1} or U_{N-1} at the new set of collocation points $\{x_i\}$:

$$U_{N\pm1}(x_i, t) = U_N(x_i, t), \quad i = 0, ..., N\pm1, \tag{2.3}$$

where U_{N+1} uses $N+2$ basis functions for refinement and U_{N-1} uses N basis functions for coarsening.

In Algorithm 1, ηf_0 is the refinement threshold such that if the current frequency indicator $f > \eta f_0$, we increase the expansion order N. The **while** loop starting in Line 9 ensures we either refine enough such that the frequency indicator, after increasing N, is smaller than the threshold ηf_0, or the maximal allowable expansion order increment within a single step $N_{\max}$ is reached.

After increasing N, f_0 is set to the current frequency indicator and η is multiplied by a factor $\gamma \geq 1$, enabling us to dynamically adjust the refinement threshold for the next refinement in order to prevent increasing N too fast without substantially increasing accuracy. On the other hand, when an extremely large N is needed to match the increasingly oscillatory behavior of the numerical solution, we can set $\gamma \succeq 1$ or even $\gamma = 1$, as we will do in Examples 6 and 9. We have observed numerically, as expected, that the larger η_0, γ are, the more difficult it is to increase the expansion order.

We also consider reducing N when a large expansion order is not really needed and f_0/η_0 is the threshold for decreasing the expansion order. If the condition in Line 17 is satisfied and $N > N_{\min}$, the minimal allowable expansion order, and we have not increased N in the current step, on the contrary we consider decreasing the expansion order below Line 17. As long as the frequency indicator of the new numerical solution with the decreased expansion order $\mathcal{F}(U_{N-1})$ is smaller than f_0, the frequency indicator recorded after previously adjusting the expansion order, reducing the expansion order is accepted; else reducing the expansion order is declined. Therefore, f_0 after coarsening will not surpass f_0 before coarsening. This procedure is described by the **If** condition in Line 22. If N is decreased, f_0 will become the latest frequency indicator. In addition, if the current frequency indicator $f \in [\frac{f_0}{\eta_0}, \eta f_0]$, neither the refinement nor the coarsening subroutine is activated.

Algorithm 1 can be generalized to higher dimensions in a dimension-by-dimension manner. The expansion order for each dimension can change simultaneously within each timestep by using the tensor product of one-dimensional basis

Table 1
Typical choices of basis functions $\{B_i\}_{i=0}^{\infty}$ and computational domain Λ.

Computational domain	Bounded interval	$(0, \infty)$	$(-\infty, \infty)$
Basis functions	Jacobi polynomials	Laguerre polynomials/functions	Hermite polynomials/functions

functions, in much the same way moving and scaling algorithms were generalized to higher dimensions [8]. For example, for a two-dimensional problem, given

$$U_{\vec{N}}(x, y) := \sum_{i=0}^{N_x} \sum_{j=0}^{N_y} u_{i,j} B_i(x) B_j(y) \tag{2.4}$$

where $\vec{N} = (N_x, N_y)$, the frequency indicator in the x-direction is defined as

$$\mathcal{F}_x(U_{\vec{N}}) := \left(\frac{\sum\limits_{i=N_x-M_x+1}^{N_x} \sum\limits_{j=0}^{N_y} \gamma_i \gamma_j u_{i,j}^2}{\sum\limits_{i=0}^{N_x} \sum\limits_{j=0}^{N_y} \gamma_i \gamma_j u_{i,j}^2} \right)^{\frac{1}{2}}, \tag{2.5}$$

while the frequency indicator in y-direction is similarly defined. At each timestep, we keep N_y fixed and use $\mathcal{F}_x$ to judge whether or not to renew $N_x \to \tilde{N}_x$; simultaneously, we fix N_x and use $\mathcal{F}_y$ to renew $N_y \to \tilde{N}_y$ if adjusting the expansion order in y dimension is needed. Finally N_x, N_y are updated to $\tilde{N}_x, \tilde{N}_y$.

In this work, the relative L^2_ω-error

$$\text{Error} = \frac{\|U_N - u\|_\omega}{\|u\|_\omega}, \tag{2.6}$$

is used to measure the quality of the spectral approximation $U_N(x)$ compared to the reference solution $u(x)$. Table 1 lists some typical choices of orthogonal basis functions for different domains Λ that we use in this paper.

We provide two examples of using this p-adaptive technique in Algorithm 1 below, where the generalized Jacobi polynomials [18] are used. Theorem 3.41 in [18] gives an estimation for the interpolation error of a function u in the Jacobi-weighted Sobolev space for $\alpha, \beta > -1$ as follows

$$\|\partial_x^\ell (I_{N,\alpha,\beta} u - u)\|_{\omega_{\alpha+\ell,\beta+\ell}} \le c\sqrt{\frac{(N-m+1)!}{N!}} N^{\ell-(m+1)/2} \|\partial_x^m u\|_{\omega_{\alpha+m,\beta+m}}, \quad 0 \le \ell \le m \le N+1, \tag{2.7}$$

where c is a positive constant independent of m, N and u. When $m > 0$ and $\ell = 0$, the left hand side becomes the interpolation error $\|(I_{N,\alpha,\beta} u - u)\|_{\omega_{\alpha,\beta}}$ which may decrease with N. Therefore, by increasing the expansion order for the Jacobi polynomials it is generally true that the interpolation will be more accurate. Theorem 7.16 and Theorem 7.17 in [18] give similar error estimates for Laguerre and Hermite interpolations, which reveals that under some smoothness assumptions, the interpolation error decreases when the expansion order N increases.

Since unbounded domain problems may involve diffusive and advective behavior, we discuss and develop adaptive spectral methods in unbounded domains in the next section.

Example 1. We numerically solve the PDE

$$\partial_t u = \left(\frac{x+2}{t+1} \right) \partial_x u, \quad x \in [-1, 1], \tag{2.8}$$

with a Dirichlet boundary condition specified at $x = 1$ given as $u(1, t) = \cos 3(t + 1)$. This PDE admits an analytical solution

$$u(x, t) = \cos((t+1)(x+2)). \tag{2.9}$$

We solve it numerically by using Chebyshev polynomials with Chebyshev-Gauss-Lobatto quadrature nodes and weights. The Chebyshev polynomials are orthogonal under the weight function $\omega(x) = (1 - x^2)^{-\frac{1}{2}}$, *i.e.*, they correspond to Jacobi polynomials with $\alpha = \beta = -\frac{1}{2}$. Since $u(x, t)$ becomes increasingly oscillatory over time, an increasing expansion order is required to capture these oscillations. We start with $N = 10$ at $t = 0$, the parameters $\eta = 1.5, \gamma = 1.1, N_{\max} = 3, N_{\min} = 0$, and a timestep $\Delta t = 0.001$. We use a third order explicit Runge-Kutta scheme to advance time.

The reference solution $u(x, t)$ is plotted in Fig. 1(a). The increasing oscillations lead to a fast rise in the frequency indicator as the contribution from high frequency modes increases. Keeping the same number of basis functions over time will fail as it will be eventually incapable of capturing the shorter wavelength oscillations.

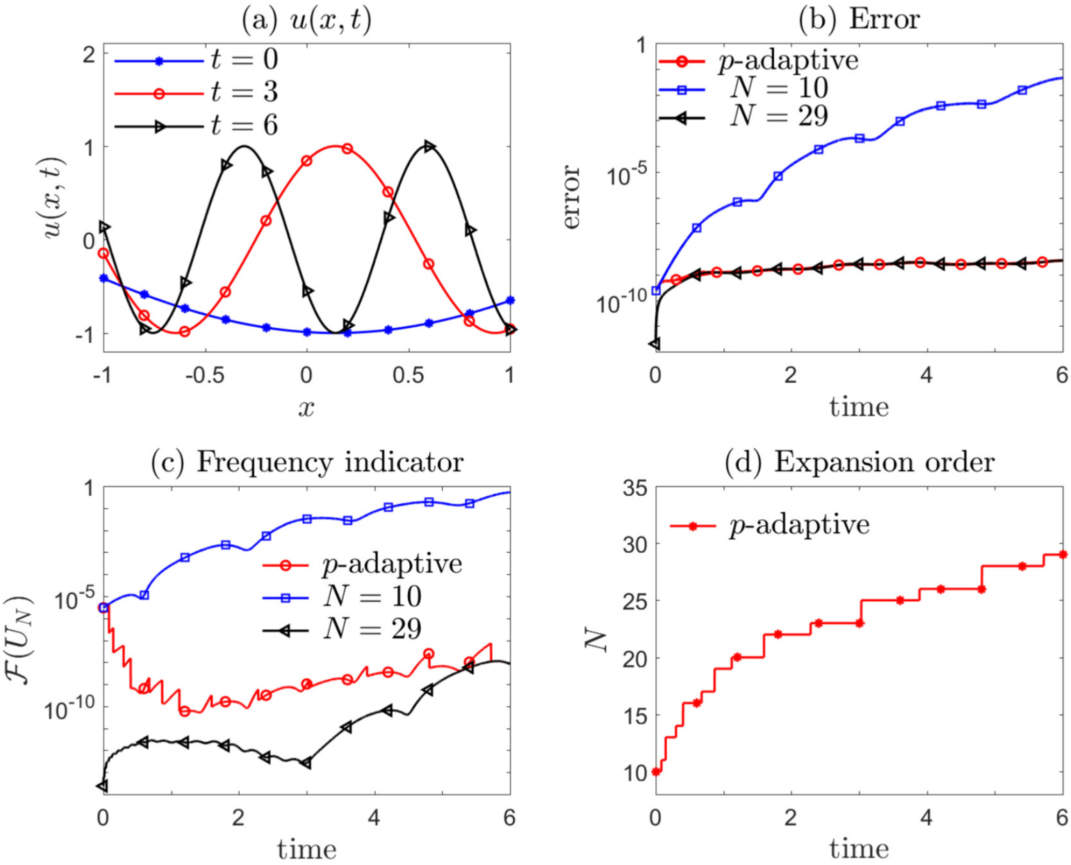

Fig. 1. Numerical solution of Eq. (2.8) with Chebyshev polynomials using Algorithm 1. For solutions that become increasingly oscillatory, the p-adaptive technique can increase the expansion order effectively to capture the oscillations and maintain a small error by keeping the frequency indicator low. A fixed $N=10$ fails to maintain the frequency indicator and results in a larger error, whereas using a fixed $N=29$, the largest expansion order appearing during the p-adaptive procedure, will not result in higher accuracy at $t=6$ than the p-adaptive technique but requires a higher computational cost. The p-adaptive technique dynamically selects an expansion order N that saves computational costs while maintaining accuracy.

However, a much more accurate approximation can be obtained (see Fig. 1(b)) with our p-adaptive method which maintains the frequency indicator (see Fig. 1(c)) by increasing the number of basis functions (shown in Fig. 1(d)). Furthermore, the coarsening subroutine for decreasing the expansion order described in the **while** loop in Line 17 will not be triggered (shown in Fig. 1(d)). The largest expansion order $N=29$ appearing during the p-adaptive procedure occurs at $t=6$. For comparison, we also plot the error and the frequency indicator for fixed $N=29$ (black curves in Figs. 1(b, c)). Using a fixed $N=29$ does not lead to a more accurate result at $t=6$ than the p-adaptive technique starting from $N=10$ because a larger expansion order is not needed when t is small. On our laptop, the solution in $t\in[0,6]$, using fixed $N=29$, took 339.0469 seconds to evaluate while p-adaptive method required only 294.9531 seconds. Therefore, the p-adaptive method maintained accuracy while requiring a lower computational cost. In this and subsequent examples, we record the runtime as a measure of computational costs. All computations were performed using MATLAB with double precision running on a laptop with a 4-core i7-8550U Intel CPU running at 1.80 GHz.

When directly approximating the reference solution in Eq. (2.9), we can achieve 10^{-8} accuracy with only 20 basis functions. However, when numerically solving Eq. (2.8), the error will accumulate due to the increasing oscillatory behavior which will require even more basis functions to achieve the same accuracy as the direct approximation to Eq. (2.9). Thus, the oscillatory behavior of the solution poses additional difficulties and requires even more refinement when numerically solving a PDE.

Next, we present an example in which we apply the proposed p-adaptive technique to approximate a function which is oscillatory over time and contains a singularity.

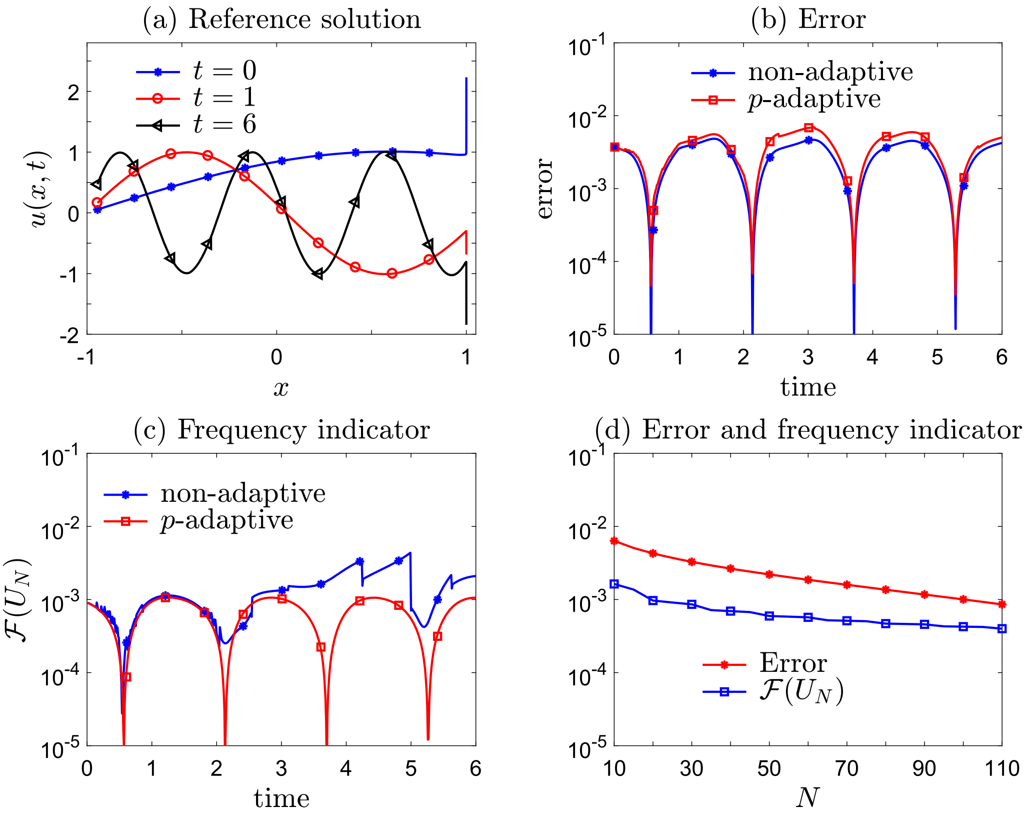

Fig. 2. The p-adaptive technique applied to evaluating the singular function in Eq. (2.10). The function $u(x, t)$ becomes more oscillatory when $t \in [0, 1] \cup [2, 6]$ and less oscillatory when $t \in [1, 2]$ and has a singularity at $x = 1$. The error of the approximation decreases very slowly with increasing expansion order due to this singularity. Applying the p-adaptive technique straightforwardly in the whole domain $[-1, 1]$ cannot substantially increase accuracy due to its failure to approximate the singularity. (For interpretation of the colors in the figure(s), the reader is referred to the web version of this article.)

Example 2. We approximate the function

$$u(x,t)=\begin{cases}(1-x)^{-0.01}\sin\left((2t+1)(x+1)\right), t\in[0,1),\\(1-x)^{-0.01}\sin\left((5-2t)(x+1)\right), t\in[1,2),\\(1-x)^{-0.01}\sin\left((2(t-2)+1)(x+1)\right), t\geq 2,\end{cases}\tag{2.10}$$

where $x \in [-1, 1]$ and $t \in [0, 6]$, by Chebyshev polynomials with Chebyshev-Gauss quadrature nodes and weights. The function carries a singularity at $x = 1$ as $\lim_{x\to 1} |u(x, t)| = +\infty$ except when t satisfies $u(1, t) = 0$. Away from the singularity, the function becomes more oscillatory in $t \in [0, 1] \cup [2, 6]$ and less oscillatory when $t \in [1, 2]$ as shown in Fig. 2(a). The expansion order should be increased or decreased appropriately when the function becomes more or less oscillatory to maintain accuracy or to relieve computational burden.

As clearly shown in [23], the error when using spectral methods to approximate $u(x, t)$ in Eq. (2.10) with the Jacobi basis functions is about 10^{-4}, as shown in Figs. 2(b, c), where we approximate Eq. (2.10) with and without the p-adaptive technique by setting the initial expansion order $N = 25$, $\eta = 1.1$ and $\gamma = 1.1$. It can be seen that directly approximating u in Eq. (2.10) leads to a large error even with the p-adaptive technique (red curve in Fig. 2(b)). Large errors are accompanied by large frequency indicators as shown in Fig. 2(c). This error cannot be significantly reduced by simply increasing the expansion order (up to $N = 110$ shown in Fig. 2(d)) because of the singularity at $x = 1$. Both the error and frequency indicator decay very slowly with increasing N due to the failure in approximating the singularity.

In order to accurately approximate $u(x, t)$, we divide the interval $x \in [-1, 1]$ into $I_\ell = [-1, 0.99)$ and $I_r = [0.99, 1]$ to isolate a small neighborhood around the singularity and approximate the function separately in the two subdomains. Fig. 3(a) plots the distribution of errors associated with approximating $u(x, 6)$ in the whole domain $[-1, 1]$ by using a fixed expansion order $N = 38$ and by using a fixed expansion order $N = 26$ in the subdomain I_ℓ and $N = 11$ in I_r. By separating the domain, the resulting errors are smaller in both subdomains. Next, we apply the p-adaptive technique in both subdomains. In I_ℓ, the function is nonsingular and its varying oscillatory behavior resulting from the factor $\sin((2t + 1)(x + 1)), t \in [0, 1)$, $\sin\left((5 - 2t)(x + 1)\right), t \in [1, 2)$ or $\sin((2(t - 2) + 1)(x + 1)), t \geq 2$ in Eq. (2.10) requires proper adjustment of the expansion order. In I_r, the function is dominated by the singular term $(1 - x)^{-0.01}$. In this two-subdomain approximation, we

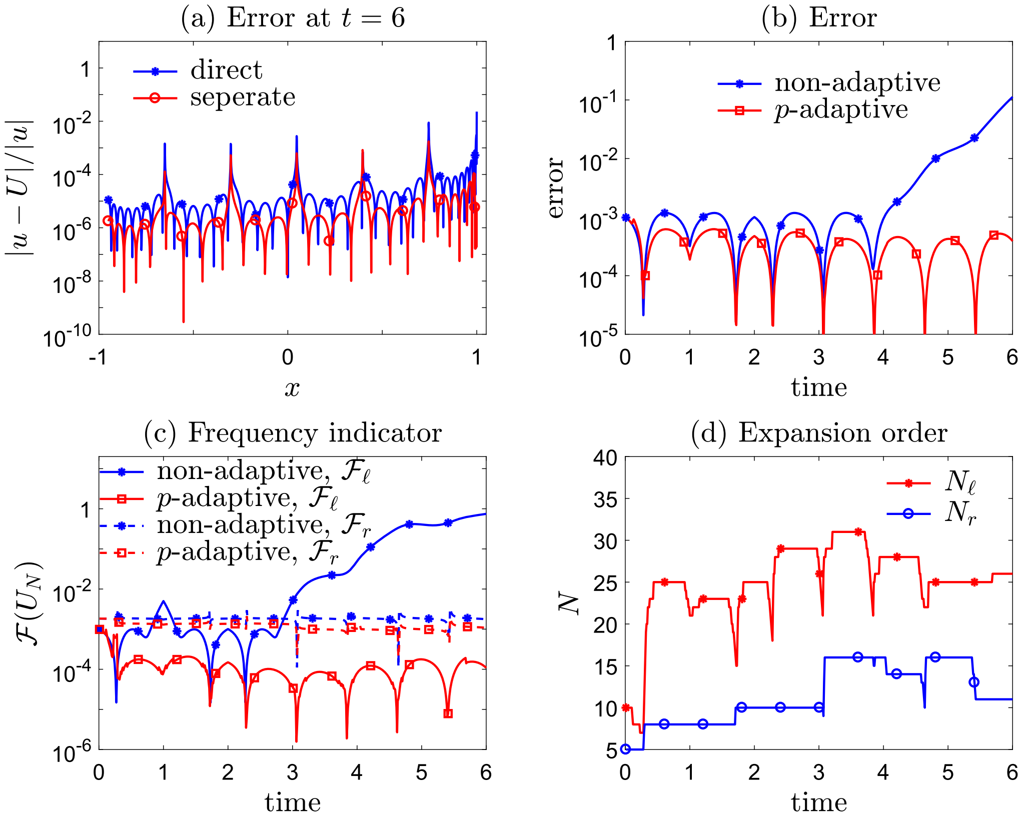

Fig. 3. Dividing the function in Eq. (2.10) into the domains $[-1, 1] = [-1, 0.99) \cup [0.99, 1]$ and using the p-adaptive technique to separately approximate $u(x, t)$ in each subdomain. Dividing the domain and separating the neighborhood of the singularity leads to improved accuracy compared to approximating $u(x, t)$ in the whole function $[-1, 1]$. In the subdomain I_ℓ, oscillatory behavior dominates and properly adjusting the expansion order N_ℓ by the p-adaptive technique is necessary (red curve in (d)). In the subdomain I_r, adjusting the expansion order N_r is not essential (blue curve with circles in (d)).

set $\eta = 1.05$, $\gamma = 1.1$, an initial expansion order $N = 10$, $N_{\max} = 15$, $N_{\min} = 0$ for the numerical solution U_ℓ in subdomain I_ℓ, and $\eta = 1.2$, $\gamma = 1.1$, an initial expansion order $N = 5$, $N_{\max} = 9$, $N_{\min} = 0$ for the numerical solution U_r in subdomain I_r. The timestep is $\Delta t = 0.01$.

Fig. 3 displays the numerical results of first dividing the domain into two subdomains $I_\ell \cup I_r$ and then approximating the function separately in each of them. As shown in Fig. 3(b), the errors for the p-adaptive methods in the subdomains I_ℓ and I_r are smaller presumably because the frequency indicators in both subdomains can be better controlled, as shown in Fig. 3(c). To approximate the varying oscillatory behavior in I_ℓ we need to adjust N_ℓ (the expansion order for U_ℓ) while to approximate $u(x, t)$ in the neighborhood of the singularity in I_r does not rely on adjusting the expansion order (Fig. 3(d)). Thus, by using this domain separation strategy to isolate the neighborhood of the singularity, the p-adaptive technique can be used to capture varying oscillatory behavior, leading to higher accuracy if the singular behavior is appropriately captured.

Finally, we present an example of a two-dimensional problem in $[-1, 1]^2$.

Example 3. We approximate the function

$$u(x, y, t) = \cos\left(xy(5 - 2|t - \tfrac{5}{2}|)\right) + y^{10-4|t-5/2|} \sin\left(4x(5 - 2|t - \tfrac{5}{2}|)\right), \ (x, y) \in [-1, 1]^2 \tag{2.11}$$

by Legendre polynomials (corresponding to Jacobi polynomials with $\alpha = \beta = 0$) with Legendre-Gauss-Lobatto quadrature nodes and weights in both dimensions. Within $t \in [0, \frac{5}{2}]$, the function becomes more oscillatory over time in both dimensions, requiring increasing expansion orders. For $t \in [\frac{5}{2}, \frac{7}{2}]$, the error for approximation with fixed expansion orders in both dimensions decreases because the function becomes less oscillatory, and therefore a reduction in expansion orders in both directions can be used to reduce computational effort without compromising accuracy. Since the function is not symmetric in x and y, the adjustment of expansion order is anisotropic. We show that Algorithm 1 can appropriately increase N_x, N_y when $t < \frac{5}{2}$ and reduce N_x, N_y when $t \geq \frac{5}{2}$. We take $N_x = N_y = 36$ at $t = 0$ with a timestep $\Delta t = 0.01$, and $\gamma_x = \gamma_y = 1.1$, $\eta_x = \eta_y = 1.1$, $N_{\max,x} = N_{\max,y} = 3$, $N_{\min,x} = N_{\min,y} = 0$. The maximum expansion orders during $t \in [0, 5]$ are $N_x = 64$ and $N_y = 51$ for the p-adaptive method, which we also use as fixed expansion orders for comparison.

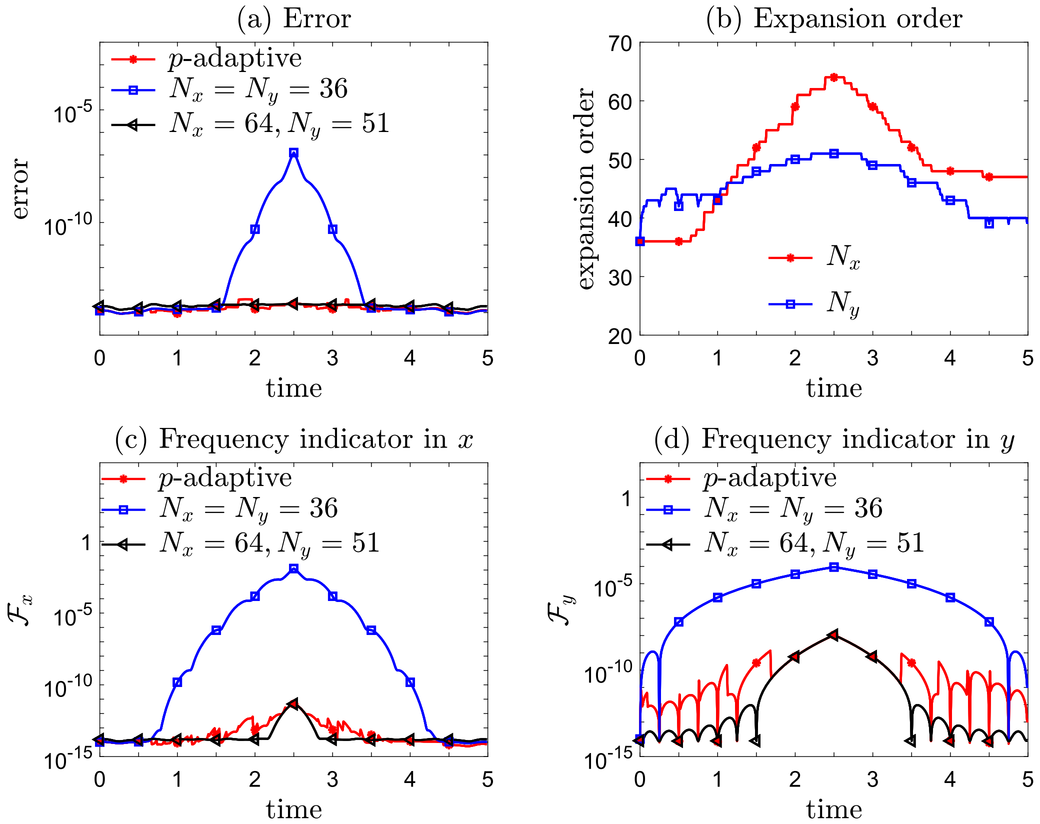

Fig. 4. Using the p-adaptive technique to approximate the two-dimensional function in Eq. (2.11) with Legendre polynomials. Refinement is applied in each direction simultaneously to capture increasing oscillations in both directions. Coarsening is applied when large expansion orders are not needed. Anisotropic oscillatory behavior requires adjusting the expansion order in each direction differently. The frequency indicators in both dimensions are kept low, leading to a small error.

It is evident from Fig. 4(a) that fixing the number of basis functions to $N_x = N_y = 37$ in each dimension leads to an approximation which deteriorates while the proposed p-adaptive spectral method is able to keep the error small. The p-adaptive technique can maintain the same accuracy as using $N_x = 64$ and $N_y = 51$, as shown in Fig. 4(a), but requires only 2.3681×10^3 seconds of run-time compared to 2.5365×10^3 seconds when using fixed $N_x = 64$, $N_y = 51$. This example confirms that the p-adaptive technique can reduce computational burden by appropriate adjustment of the expansion order. Furthermore, when $t \in [\frac{5}{2}, 5]$ we see that with fixed expansion orders $N_x = 64$ and $N_y = 51$ the approximation error decreases, indicating that coarsening can be tolerated to relieve computational burden while maintaining accuracy. Algorithm 1 first tracks increasing oscillations by increasing expansion orders in both x and y directions. When $t \geq \frac{5}{2}$, Algorithm 1 senses a decrease in the frequency indicator and decreases both N_x and N_y adaptively (Fig. 4(b)) without compromising accuracy (blue and black curves in Fig. 4(a)). Overall, Algorithm 1 preserves accuracy for all times while avoiding excessive values of N_x and N_y when they are not needed.

Since $\sin(4x(5 - 2|t - \frac{5}{2}|))$ is the most oscillatory term in $u(x, y, t)$, the function is more oscillatory in x than in y for $t \in [0, \frac{5}{2}]$. Therefore, the expansion orders should be adjusted anisotropically and we expect N_x needs to be increased more than N_y in order to keep $\mathcal{F}_x$ small, which is indeed observed (Fig. 4(b)). That is, the proposed p-adaptive technique can successfully sense the function's heterogeneity and adjust the expansion orders differently in each dimension. Over time, both $\mathcal{F}_x$ and $\mathcal{F}_y$ in the p-adaptive approximation are maintained as well as when $N_x = 64$ and $N_y = 51$ are fixed (Figs. 4(c, d)), leading to satisfactory error control.

3. Adaptive spectral methods in unbounded domains

Unbounded domain problems are often more difficult to solve numerically than bounded domain problems. Diffusion and advection in unbounded domains necessitates knowledge of the solution's behavior at infinity. To distinguish and handle diffusive and advective behavior in unbounded domains, techniques for scaling and moving basis functions are proposed in [8]. When combining scaling, moving, refinement and coarsening, we can devise a comprehensive adaptive spectral approach for unbounded domains. A flow chart of our overall approach is given in Fig. 5. The scaling, refinement and coarsening techniques all rely on a common frequency indicator.

Algorithm 2 Pseudo-code of the frequency-dependent scaling technique which adjusts the scaling factor β.

```
$f \leftarrow$ FREQUENCY_INDICATOR($U_N^{(\alpha,\beta)}(t+\Delta t)$)
if $f > \nu f_1$ then    # try decreasing $\beta$
    $\tilde{\beta} \leftarrow q\beta$
    $U_N^{(\alpha,\tilde{\beta})} \leftarrow$ SCALE($U_N^{(\alpha,\beta)}(t+\Delta t), \tilde{\beta}$)
    $\tilde{f} \leftarrow$ FREQUENCY_INDICATOR($U_N^{(\alpha,\tilde{\beta})}$)
    while $\tilde{f} \le f$ and $\tilde{\beta} \ge \underline{\beta}$ do
        $\beta \leftarrow \tilde{\beta}$
        $U_N^{(\alpha,\beta)}(t+\Delta t) \leftarrow U_N^{(\alpha,\tilde{\beta})}$
        $f_1 \leftarrow \tilde{f}$
        $f \leftarrow \tilde{f}$
        $\tilde{\beta} \leftarrow q\beta$
        $U_N^{(\alpha,\tilde{\beta})} \leftarrow$ SCALE($U_N^{(\alpha,\beta)}(t+\Delta t), \tilde{\beta}$)
        $\tilde{f} \leftarrow$ FREQUENCY_INDICATOR($U_N^{(\alpha,\tilde{\beta})}$)
    end while
else if $f < f_1$ then    # try increasing $\beta$
    $\tilde{\beta} \leftarrow \beta/q$
    $U_N^{(\alpha,\tilde{\beta})} \leftarrow$ SCALE($U_N^{(\alpha,\beta)}(t+\Delta t), \tilde{\beta}$)
    $\tilde{f} \leftarrow$ FREQUENCY_INDICATOR($U_N^{(\alpha,\tilde{\beta})}$)
    while $\tilde{f} \le f$ and $\tilde{\beta} \le \overline{\beta}$ do
        $\beta \leftarrow \tilde{\beta}$
        $U_N^{(\alpha,\beta)}(t+\Delta t) \leftarrow U_N^{(\alpha,\tilde{\beta})}$
        $f_1 \leftarrow \tilde{f}$
        $f \leftarrow \tilde{f}$
        $\tilde{\beta} \leftarrow \beta/q$
        $U_N^{(\alpha,\tilde{\beta})} \leftarrow$ SCALE($U_N^{(\alpha,\beta)}(t+\Delta t), \tilde{\beta}$)
        $\tilde{f} \leftarrow$ FREQUENCY_INDICATOR($U_N^{(\alpha,\tilde{\beta})}$)
    end while
end if
```

As is stated in [8], advection may cause a false increase in the frequency indicator. Thus, we must first compensate for advection by the moving technique before we consider either scaling or adjusting the expansion order. Next, as the cost of changing the scaling factor is lower than increasing the expansion order, we implement scaling before adjusting the expansion order. Only if scaling cannot maintain the frequency indicator below the refinement threshold do we consider increasing the expansion order. Coarsening is also considered after scaling if the frequency indicator decreases below the threshold.

As was done in [8], we also decrease the scaling factor β by multiplying it by a common ratio $q < 1$ if the current frequency indicator is larger than the scaling threshold $f > \nu f_1$. The scaling we perform here contains an additional step: when the current frequency indicator decreases and is below f_1, we consider increasing the scaling factor β by dividing it by the common ratio q as long as the frequency indicator decreases after increasing β. When $f \in [f_1, \nu f_1]$, β is neither increased nor decreased. Thus, at each step, the scaling factor β may be either increased or decreased as long as the frequency indicator decreases after adjusting the scaling factor. A decrease in the scaling factor indicates that the allocation points are more efficiently distributed. These changes avoid unnecessary computational burden that may arise if N is excessively increased. We briefly describe our modified scaling subroutine for one timestep in Algorithm 2.

For simplicity, we assume that the function is moving rightward so we need to move the basis functions rightward. Therefore, (x_R, ∞) is the "exterior domain" of the spectral approximation on which we wish to control the error as illustrated in [8]. For Laguerre polynomials/functions the parameter x_L in the algorithm in Fig. 5 denotes the starting point for the approximation, while for Hermite polynomials/functions x_L represents the translation of Hermite polynomials/functions, *i.e.*, we use $\{\mathcal{H}_i(x-x_L)\}$ or $\{\hat{\mathcal{H}}_i(x-x_L)\}$. Let $U_{N,x_L}^{(\beta)}$ be the spectral approximation with the scaling factor β. The exterior-error indicator for the semi-unbounded domain is defined in [8] and we can generalize it to $\mathbb{R}$ when using Hermite polynomials/functions

$$\mathcal{E}(U_{N,x_L}^{(\beta)}, x_R) = \frac{\|\partial_x U_{N,x_L}^{(\beta)} \cdot \mathbb{I}_{(x_R,+\infty)}\|_{\omega_\beta}}{\|\partial_x U_{N,x_L}^{(\beta)} \cdot \mathbb{I}_{(-\infty,+\infty)}\|_{\omega_\beta}}, \tag{3.1}$$

where ω_β is the weight function and x_R is taken to be $x^{(\beta)}_{[\frac{2N+2}{3}]}$ for Hermite functions/polynomials and $x^{(\alpha,\beta)}_{[\frac{N+2}{3}]}$ for Laguerre functions/polynomials [8] in view of the often-used $\frac{2}{3}$-rule. The difference between the choices of x_R for Hermite and Laguerre basis functions arises because the allocation points for Hermite functions are symmetrically distributed around their center while those for Laguerre functions are one-sided, to the right of the starting point x_L in the axis. If the solution $u(x)$ moves rightward in time, the spectral approximation at large distances may deteriorate and the exterior-error indicator

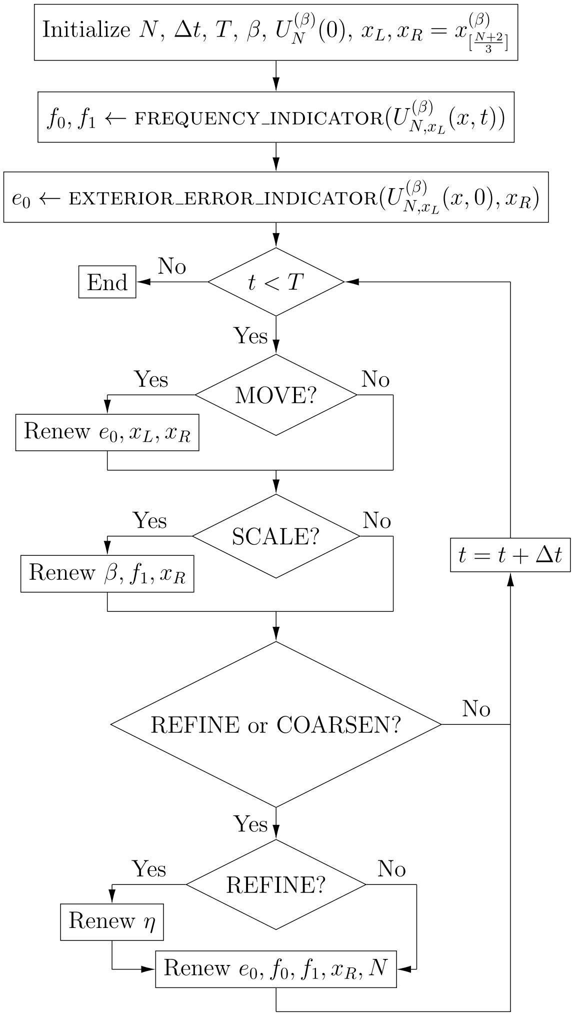
Initialize N, Δt, T, β, $U_N^{(\beta)}(0)$, $x_L, x_R = x^{(\beta)}_{[\frac{N+2}{3}]}$
$f_0, f_1 \leftarrow$ FREQUENCY_INDICATOR($U^{(\beta)}_{N,x_L}(x,t)$)
$e_0 \leftarrow$ EXTERIOR_ERROR_INDICATOR($U^{(\beta)}_{N,x_L}(x,0), x_R$)
End
No
$t < T$
Yes
Yes
MOVE?
No
Renew e_0, x_L, x_R
Yes
SCALE?
No
Renew β, f_1, x_R
$t = t + \Delta t$
REFINE or COARSEN?
No
Yes
Yes
REFINE?
No
Renew η
Renew e_0, f_0, f_1, x_R, N

Fig. 5. Flow chart of an adaptive spectral method in unbounded domains that includes moving, scaling, refinement and coarsening techniques.

$\mathcal{E}(U^{(\beta)}_{N,x_L}, x_R)$ will increase. This means that the moving mechanism will be triggered and the starting point of the spectral approximation will need to be updated by $x_L \to x_L + d_0$ with the displacement determined by $d_0 = \min\{n\delta, d_{\max}\}$. Here n is the smallest integer satisfying $\mathcal{E}(U^{(\beta)}_{N,x_L}, x_R + n\delta) < \mu e_0$, δ is the minimum displacement, $d_{\max}$ is the maximum displacement, and μ represents the threshold of the increase in the exterior-error indicator (the current value of which is given by e_0) that we can tolerate.

For the scaling subroutine we need the following parameters: the common ratio $q < 1$ that we use to geometrically shrink/increase the scaling factor, the parameter describing the threshold for considering shrinking the scaling factor ν; a predetermined lower bound for the scaling factor $\underline{\beta}$ and an upper bound $\overline{\beta}$. For the moving subroutine, required parameters include the minimal displacement for the moving technique δ, the maximal displacement within a single timestep $d_{\max}$, and the parameter of the threshold for activating the moving technique μ. At $t = 0$, we ensure the frequency indicator and the exterior-error indicator are relatively small by choosing a suitable initial scaling factor β and an appropriate initial translation of basis functions x_L, respectively.

The SCALE and MOVE tests are shown in Fig. 5 while EXTERIOR_ERROR_INDICATOR calculates the exterior-error indicator for the moving subroutine. A detailed discussion on the scaling and moving techniques is given in [8]. Note that after the expansion order N has changed, we need to renew the threshold for scaling, the threshold for subsequent adjustment of the expansion order, as well as the threshold for moving, as indicated in Fig. 5. After first applying the moving technique, adjusting the expansion order and scaling both depend on the frequency indicator and aim to keep the frequency indicator low to control the error. The relationship and interdependence between them is key to understanding and justifying the first-scaling-then-adjusting expansion-order procedure in Fig. 5. Thus, we need to investigate how the proposed scaling technique will affect our p-adaptive technique and how these two techniques interact with each other. We use two examples containing both diffusive and oscillatory behavior to investigate how the two techniques will be activated and influence each

Table 2
Error, β, and N at $t = 5$ for different η and γ with both p-adaptive and scaling techniques.

η γ	1.2	1.5	2	4
1.05	1.434, 67 1.305e-05	1.434, 64 2.346-05	1.362, 58 7.687e-05	2.053, 55 6.030e-05
1.1	1.510, 62 2.500e-05	1.434, 69 5.396e-05	1.673, 66 5.513e-05	2.053, 55 6.030e-05
1.2	1.853, 56 4.451e-05	1.673, 56 5.512e-05	1.673, 53 8.927e-05	1.853, 53 8.706e-05
1.5	1.589, 52 1.369e-04	1.673, 53 8.927e-05	1.761, 52 1.099e-04	1.951, 53 8.702e-05

Table 3
Error and N at $t = 5$ for different η and γ with the p-adaptive technique but without the scaling technique, $\beta = 4$.

η γ	1.2	1.5	2	4
1.05	79 1.316e-05	71 3.720e-05	65 9.724e-05	59 2.364e-04
1.1	70 4.372e-05	67 6.544e-05	64 9.823e-05	58 2.607e-04
1.2	65 9.724e-05	62 1.534e-04	61 1.597e-04	58 2.607e-04
1.5	59 2.364e-03	59 2.364e-04	58 2.607e-04	56 3.508e-04

other. In Example 4, both refinement and reducing β are needed for matching increasing oscillatory and diffusive behavior of the solution; in Example 5, a less oscillatory and diffusive solution over time implies that coarsening and increasing β may be considered.

Example 4. We approximate the function

$$u(x,t) = \exp\left[-\frac{x}{(bt+a)}\right]\cos x, \quad t \in \mathbb{R}^+ \tag{3.2}$$

with the generalized Laguerre function basis $\{\hat{\mathcal{L}}_i^{(\alpha,\beta)}(x)\}_{i=0}^{\infty}$ discussed in [8] with the parameter $\alpha = 0$. The magnitude of oscillations for this function, $\exp(-\frac{x}{(bt+a)})$, increases over time, requiring proper scaling. Under a variable transformation $y = \frac{x}{bt+a}$, $u(x,t)$ can be rewritten as $u(y,t) = \cos((bt+a)y)\exp(-y)$, indicating that the solution is increasingly oscillatory in y as time increases. Thus, if we reduce the scaling factor β to match the diffusive behavior of the solution, proper refinement is also required. In other words, diffusive and oscillatory behavior is coupled in this example. We carry out numerical experiments using the algorithm described in Fig. 5 with different (η, γ) to investigate how scaling and refinement influence each other. We deactivate the moving technique by setting $d_{\max} = 0$ since the solution exhibits no intrinsic advection. Even if we had allowed moving, it was hardly activated. We set $\Delta t = 10^{-3}$, $N = 50$ at $t = 0$ and $a = 2, b = 0.7$. $q = \nu^{-1} = 0.95$, $\underline{\beta} = 0.3$, $\overline{\beta} = 10$, $N_{\min} = 0$, $N_{\max} = 3$ and choose the initial scaling factor $\beta = 4$.

In Tables 2 and 3 the error in $\mathbb{R}^+$ is recorded in the lower-left part of each entry while the scaling factor β and expansion order N at $t = 5$ is recorded in the upper-right. By comparing entries in each column/row for smaller η, γ, both tables show the expansion order N is likely to be increased more when the threshold for refinement ηf_0 is lower.

We see from Table 2 that with more refinement β tends to be smaller. This interaction between p-adaptivity and scaling arises because more refinement leads to a larger expansion order N and a smaller scaling threshold νf_1. Since scaling will only be performed if the frequency indicator after scaling decreases, proper refinement is not likely to lead to over-scaling. Moreover, by comparing N at $t = 5$ between Tables 2 and 3, we see that N tends to be smaller with the scaling technique for the same γ, η. This implies that without scaling, the refinement procedure is more often activated, leading to a larger N to compensate for the incapability of scaling alone to maintain a low frequency indicator. This results in a larger computational burden without an improvement in accuracy. This behavior has been expected from the design of Algorithm 5 since we put scaling before refinement so that redistribution of collocation points is tried first to avoid unnecessary refinement when the increase in frequency indicator results from diffusion instead of oscillation.

Example 5. We approximate the function

$$u(x,t) = \exp[-(bt+a)x]\cos x, \quad x, t \in \mathbb{R}^+ \tag{3.3}$$

Table 4
Error, β and N at $t = 5$ for different η_0 and γ with/without scaling for the p-adaptive technique.

η	1.2	1.5	2	4
Scaled	5.728, 11 6.514e-10	7.032, 13 8.885e-12	6.347, 13 1.260e-11	6.681, 17 1.255e-14
Unscaled	4, 20 2.707e-12	4, 28 8.127e-11	4, 31 9.417e-15	4, 30 9.672e-15

with the generalized Laguerre function basis with the parameter $\alpha = 0$. The magnitude of oscillations for this function, $\exp(-(bt + a)x)$, decreases over time and increasing the scaling factor β to more densely redistribute the allocation points is needed. Furthermore, under the variable transformation $y = (bt + a)x$, $u(x, t)$ can be rewritten as $u(y, t) = \cos(\frac{y}{bt+a})\exp(-y)$. Since the oscillations decrease with y, one can reduce the expansion order. We consider coarsening with or without scaling to investigate whether increasing β can facilitate coarsening (and save computational effort) or result in higher accuracy. We carry out numerical experiments using the algorithm described in Fig. 5 and different (η, γ) and also deactivate the moving technique by setting $d_{\max} = 0$ since the solution exhibits no intrinsic advection. We set $\Delta t = 10^{-3}$, $N = 50$ at the beginning and set the parameters $a = b = 1/2$, $q = \nu^{-1} = 0.95$, $\underline{\beta} = 0.3$, $\overline{\beta} = 10$, $N_{\min} = 0$, $N_{\max} = 3$ and initial scaling factor $\beta = 4$. We use a different threshold η_0 for coarsening and we have checked numerically that the parameter γ in the refinement subroutine will not affect the coarsening subroutine in this example.

In Table 4 the error in $\mathbb{R}^+$ is recorded in the lower-left part of each entry while the scaling factor β and expansion order N at $t = 5$ is recorded in the upper-right. By comparing entries in each row we see that a smaller η_0 will lead to easier coarsening and a smaller N at $t = 5$. Since the approximation with larger N is always better, whether we can achieve the same level of accuracy with a smaller expansion order N if proper scaling is implemented is of interest. The initial approximation error is 1.960×10^{-9} and the approximation will not worsen after coarsening regardless of η_0 because in the p-adaptive subroutine coarsening is allowed only when the post-coarsening frequency indicator remains below the previous threshold f_0. Moreover, by comparing the two rows in Table 4 we see that if the solution concentrates and becomes less diffusive, increasing β and more efficiently redistributing the allocation points allows the scaling technique to achieve high accuracy with fewer expansion orders than without the scaling technique.

The time-dependent errors and expansion orders are plotted in Fig. 6 where the p-adaptive method is compared with the non-p-adaptive method when scaling is applied. From Figs. 6(a, c) we can observe that both scaled and unscaled methods maintain the error below the initial approximation error. Yet, upon comparing Fig. 6(b) to Fig. 6(d) it is readily seen that the scaled method leads to appropriate coarsening while succeeding in maintaining low error, but the unscaled method will increase N when increasing the expansion order is not actually needed, resulting in additional unnecessary computational burden. In Fig. 6(e) the scaled and p-adaptive spectral method with $\eta_0 = 4$ is compared with the scaling-only spectral method. We see that the errors for both methods are almost the same but the p-adaptive method can reduce unnecessary computation by decreasing N adaptively while still maintaining a low error, and the approximation error for the p-adaptive method fluctuates due to a decreasing N. Fig. 6(f) shows that the scaling factor β is increased more in the p-adaptive method, implying that the reason why the p-adaptive method can achieve the same accuracy as non-p-adaptive method with a smaller expansion order is that it can redistribute the allocation points more efficiently. Finally, we conclude that all three methods: scaling, p-adaptive+scaling, and p-adaptive methods can maintain the error well below the initial approximation error, but the combined p-adaptive+scaling method can achieve this with the smallest expansion order and is therefore the most efficient method among them.

4. Applications in solving the Schrödinger equation

In this section, we apply our adaptive spectral methods described in Fig. 5 to solve Schrödinger's equation in unbounded domains

$$i\partial_t \psi(x,t) = -\partial_x^2 \psi(x,t) + V(x)\psi(x,t) + V_{\mathrm{ex}}(x,t)\psi(x,t), \quad x \in \mathbb{R}, \tag{4.1}$$

which is equivalent to the PDE discussed in [14]

$$i\partial_t u(x,t) = \Big[-(\partial_x + iA(x,t))^2 + V(x,t)\Big]u(x,t) \tag{4.2}$$

under the transformation $u(x,t) = e^{i\int_0^t V_{\mathrm{ex}}(x,s)\mathrm{d}s}\psi(x,t)$. Here, we shall use spectral methods with the Hermite function basis. The solution is complex, so in the spectral decomposition the coefficients of the basis functions are complex. The major difference here is that in [14], Schrödinger's equation is solved in a bounded domain (x_-, x_+) with absorbing boundary conditions. Using spectral methods, we are able to solve Schrödinger's equation without truncating the domain.

We solve the weak form of Eq. (4.1)

$$(\partial_t \psi, v) = -i(\partial_x \psi, \partial_x v) - i((V(x) + V_{\mathrm{ex}}(x,t))\psi, v), \quad v \in L^2(-\infty, \infty), \tag{4.3}$$

which is to find $\Psi^{\beta}_{N,x_L}(t,x) := \sum_{i=0}^{N} \psi^{\beta}_{i,x_L}(t)\hat{\mathcal{H}}^{\beta}_i(x - x_L)$ in $V^{\beta}_{N,x_L} = \mathrm{span}\{\hat{\mathcal{H}}^{\beta}_i(x - x_L)\}_{i=0}^{N}$ satisfying the initial condition and

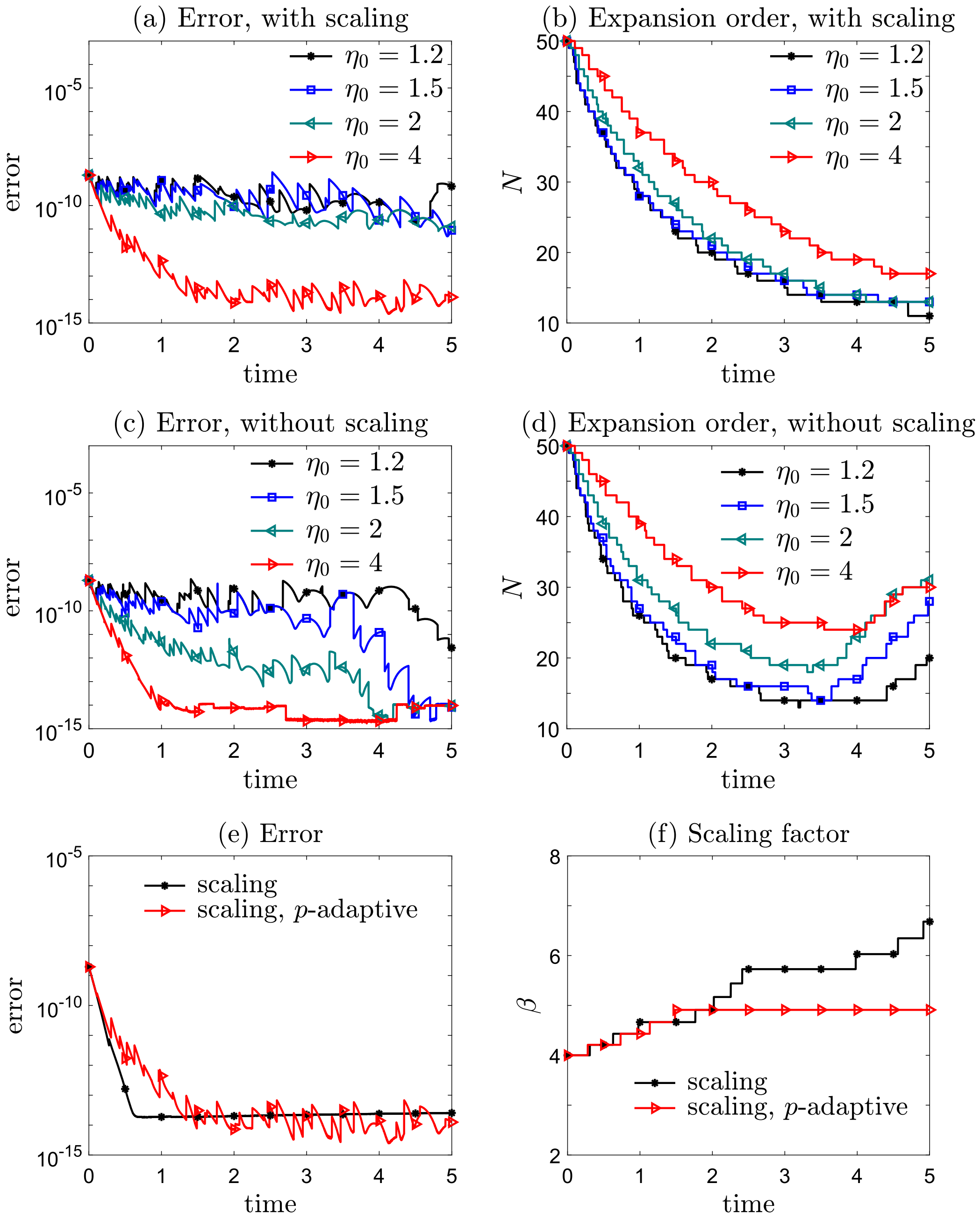

Fig. 6. Approximation to Eq. (3.3) with scaling and p-adaptive techniques. Increasing β by scaling can save computational burden while maintaining accuracy by more efficiently redistributing allocation points. The approximation error is controlled below the initial approximation error for both scaled and unscaled p-adaptive methods, but the expansion order of the scaled method is smaller. On the other hand, adjusting the scaling factor without decreasing N will not achieve higher accuracy.

$$(\partial_t \Psi^{\beta}_{N,x_L}, v) + i(\partial_x \Psi^{\beta}_{N,x_L}, \partial_x v) = -i((V(x) + V_{\mathrm{ex}}(x,t))\Psi_{N,x_L}, v), \quad \forall v \in V^{\beta}_{N,x_L}. \tag{4.4}$$

We denote $\boldsymbol{\psi}^{\beta}_{N,x_L}(t) := (\psi^{\beta}_{0,x_L}(t), \ldots, \psi^{\beta}_{N,x_L}(t))$, which can be analytically solved to advance time

$$\boldsymbol{\psi}^{\beta}_{N,x_L}(t_{n+1}) = \exp\left[-i\int_{t_n}^{t_{n+1}} (D^{\beta}_N + V^{\beta}_{N,x_L}(t))\mathrm{d}t\right]\boldsymbol{\psi}^{\beta}_{N,x_L}(t_n) \tag{4.5}$$

where $D^{\beta}_N \in \mathbb{R}^{(N+1)\times(N+1)}$ is a symmetric matrix with entries

$$(D_N^{\beta})_{\ell j} = \begin{cases} -\beta^2\sqrt{\ell(\ell+1)} & j=\ell+2, \\ -\beta^2\sqrt{(\ell-2)(\ell-1)} & j=\ell-2, \\ \beta^2\dfrac{\ell}{2} & j=\ell, \\ 0 & \text{otherwise}, \end{cases} \tag{4.6}$$

and the matrix $V_{N,x_L}^{\beta}(t) \in \mathbb{R}^{(N+1)\times(N+1)}$ has entries

$$(V_{N,x_L}^{\beta}(t))_{\ell j} = \int_{-\infty}^{\infty} (V(x)+V_{\text{ex}}(x,t))\hat{\mathcal{H}}_{\ell-1}^{\beta}(x-x_L)\hat{\mathcal{H}}_{j-1}^{\beta}(x-x_L)\mathrm{d}x. \tag{4.7}$$

The evaluation of $\exp(-i\int_{t_n}^{t_{n+1}}(D_N^{\beta}+V_{N,x_L}^{\beta}(t))\mathrm{d}t)\boldsymbol{\psi}_{N,x_L}^{\beta}(t_n)$ is performed as follows. First, we denote $\tilde{V}_{N,x_L}^{\beta} \approx \int_{t_n}^{t_{n+1}} V_{N,x_L}^{\beta}(t)\mathrm{d}t$ where the integration is evaluated by Gauss-Legendre formula. Therefore, when calculating the matrix-vector product $\tilde{V}_{N,x_L}^{\beta}\mathbf{X}_N$ for a vector $\mathbf{X}_N := (X_1, ..., X_N) \in \mathbb{R}^{N+1}$, its ℓ^{th} component is

$$\begin{aligned}(\tilde{V}_{N,x_L}\mathbf{X}_N)_{\ell} = \sum_{j=0}^{N}\sum_{s=0}^{N}\hat{H}_{\ell-1}^{\beta}(x_s^{\beta})\hat{H}_j^{\beta}(x_s^{\beta})\Big[&V(x_s^{\beta}+x_L)+\tfrac{5}{18}V_{\text{ex}}(x_s^{\beta}+x_L,t_n+\tfrac{1}{2}(1-\sqrt{\tfrac{3}{5}})\mathrm{d}t) \\ &+\tfrac{4}{9}V_{\text{ex}}(x_s^{\beta}+x_L,t_n+\tfrac{\mathrm{d}t}{2})+\tfrac{5}{18}V_{\text{ex}}(x_s^{\beta}+x_L,t_n+\tfrac{1}{2}(1+\sqrt{\tfrac{3}{5}})\mathrm{d}t)\Big]X_j\Delta t\end{aligned} \tag{4.8}$$

where $\Delta t = t_{n+1}-t_n$. We can first calculate

$$\begin{aligned}\sum_{j=0}^{N}\hat{H}_j^{\beta}(x_s^{\beta})\Big[&V(x_s^{\beta}+x_L)+\tfrac{5}{18}V_{\text{ex}}(x_s^{\beta}+x_L,t_n+\tfrac{1}{2}(1-\sqrt{\tfrac{3}{5}})\mathrm{d}t) \\ &+\tfrac{4}{9}V_{\text{ex}}(x_s^{\beta}+x_L,t_n+\tfrac{\mathrm{d}}{2})+\tfrac{5}{18}V_{\text{ex}}(x_s^{\beta}+x_L,t_n+\tfrac{1}{2}(1+\sqrt{\tfrac{3}{5}})\mathrm{d}t)\Big]X_j\Delta t\end{aligned} \tag{4.9}$$

for each subindex s; then, evaluating $(\tilde{V}_{N,x_L}^{\beta}\mathbf{X}_N)_{\ell}$ for each subindex ℓ will only require an $O(N)$ operation. In this way, given any arbitrary potentials $V(x), V_{\text{ex}}(x,t)$ we can calculate $\tilde{V}_{N,x_L}^{\beta}\mathbf{X}_N$ in $O(N^2)$ operations without explicitly calculating entries in $\tilde{V}_{N,x_L}^{\beta}$. We approximate the matrix-vector product $\exp\left[-i(D_N^{\beta}\Delta t+\tilde{V}_{N,x_L})\right]\boldsymbol{\psi}_{N,x_L}^{\beta}(t_n)$ by rewriting $\exp\left[-i(D_N\Delta t+\tilde{V}_{N,x_L})\right]\boldsymbol{\psi}_{N,x_L}^{\beta}(t_n) = \exp\left[-\frac{1}{m}i(D_N\Delta t+\tilde{V}_{N,x_L})\right]^m\boldsymbol{\psi}_{N,x_L}^{\beta}(t_n)$, which is introduced as the "scaling and squaring" method in [19], and approximate the matrix-vector product $\exp\left[-\frac{1}{m}i(D_N\Delta t+\tilde{V}_{N,x_L})\right]\mathbf{X}_N$ by truncating the infinite Taylor expansion series $\sum_{j=0}^{\infty}\frac{1}{m^j j!}\left[-i(D_N\Delta t+\tilde{V}_{N,x_L})\right]^j\mathbf{X}_N$. Here, we take $m=3$.

As mentioned in Section 1, two main numerical difficulties when solving Schrödinger's equation are the unboundedness and the oscillatory behavior of the solutions. In fact, the solution may be increasingly oscillatory behavior at infinity over time, making it very hard to solve in the unbounded domain. However, with our adaptive spectral methods, we can efficiently solve Schrödinger's equation in unbounded domains accurately and capture these oscillations.

We now revisit the examples of linear Schrödinger's equations discussed in [14], nonlinear Schrödinger's equations discussed in [24], and their semiclassical limits studied in [25]. In the following examples, curves labeled "adaptive" indicate that scaling, moving, and p-adaptive techniques are all applied as described in Fig. 5, while curves labeled "non-adaptive" indicate none of the three adaptive techniques is applied. Results obtained by applying some of the three techniques are marked by curves named by the corresponding techniques that are applied.

Example 6. We numerically solve the Schrödinger's equation which was considered in Example 1 of [14] and take $V = V_{\text{ex}} = 0$ in Eq. (4.1), admitting the analytic solution

$$\Psi(x,t) = \frac{1}{\sqrt{\zeta+it}}\exp\left[ik(x-kt)-\frac{(x-2kt)^2}{4(\zeta+it)}\right], \tag{4.10}$$

where k is related to the propagation speed of the beam and ζ determines the width of the beam. The absolute values of the real part of $\Psi(x,t=0,0.5,1)$ are plotted in Fig. 7(a), illustrating the increasingly oscillatory and diffusive behavior in the rightward propagating solution. Treatment of this solution will thus require scaling, moving, and p-adaptive techniques. The imaginary parts of the reference solution (not plotted) over time are also increasingly oscillatory. We shall apply the algorithm described in Fig. 5. We set $\zeta = 0.3, k = 1$, and initialize $N = 50$ at $t = 0$. Other parameters are set to $q = \nu^{-1} =$

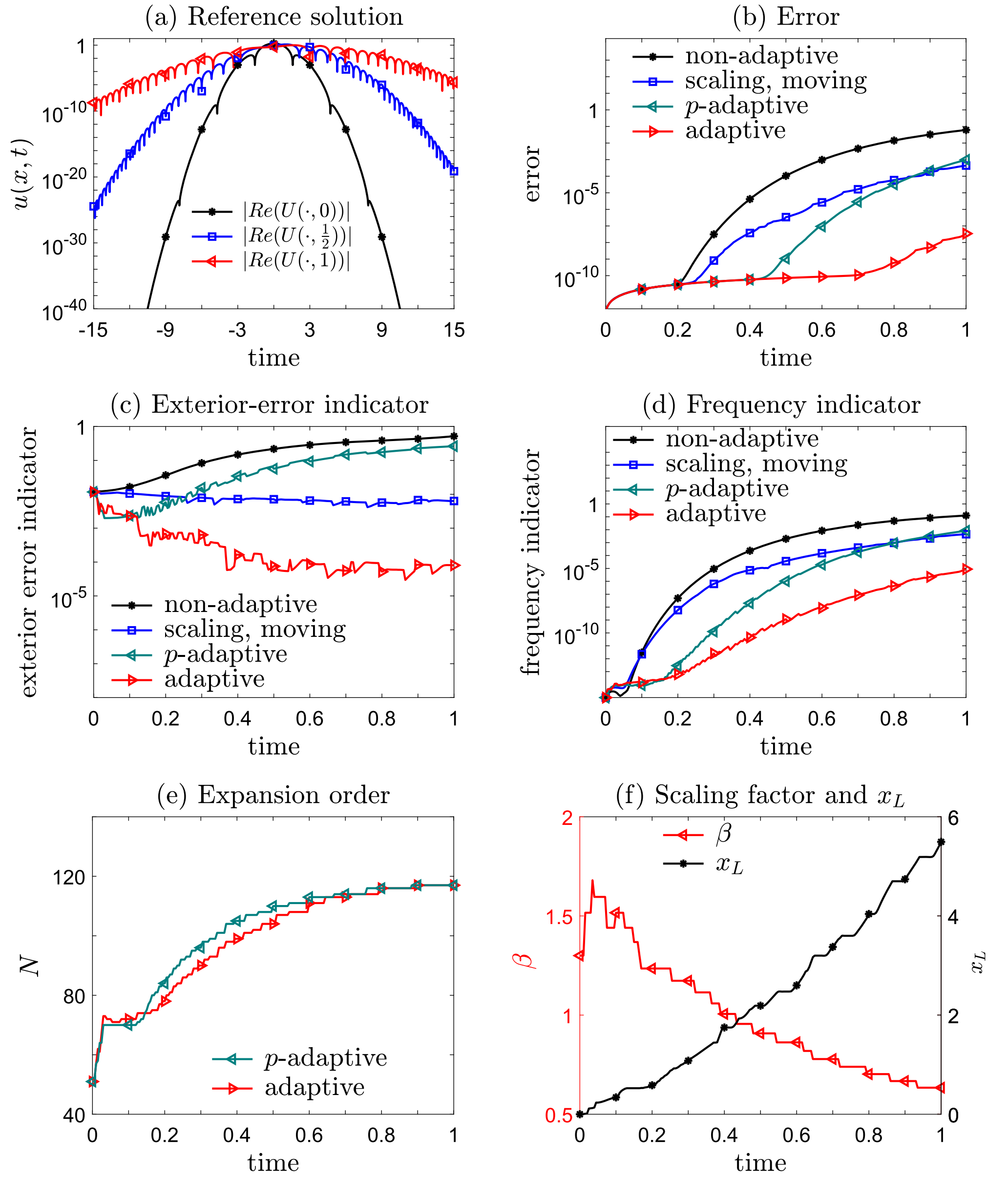

Fig. 7. Numerical solution of Schrödinger's equation with vanishing potentials. Applying scaling, moving, and p-adaptive techniques can successfully capture diffusive advective, and oscillatory behavior of the solution and yields an accurate numerical solution that prevents the frequency indicator from growing too fast. The exterior-error indicator is also kept small by moving the basis functions rightward to avoid a deteriorating approximation at ∞. Failure to incorporate any of the moving, scaling, or p-adaptive techniques results in a much larger error.

0.95, $\mu = 1.0002, d_0 = 0.005, \underline{\beta} = 0.3, \overline{\beta} = 2, d_{\max} = 0.1, N_{\max} = 6, N_{\min} = 0, \eta = 1.1, \gamma = 1.05$, and $\Delta t = 0.005$. Note that with zero potential, Eq. (4.5) reduces to

$$\boldsymbol{\psi}_N^{\beta}(t_{n+1}) = \exp\left[-iD_N^{\beta}\mathrm{d}t\right]\boldsymbol{\psi}_N^{\beta}(t_n). \tag{4.11}$$

When all four techniques are applied, the error is the smallest (shown in Fig. 7(b)) since we can keep the exterior error indicator in (x_R,∞) small (shown in Fig. 7(c)) by matching the solution's intrinsic advection. We can simultaneously prevent the frequency indicator from growing too fast (shown in Fig. 7(d)), thus ensuring a small error bound.

From the reference solution one observes that increasing the expansion order over time is an intrinsic requirement and failure to do so prevents the capture of the increasing oscillations, leading to a huge error. As the function becomes increasingly oscillatory as $x \to \infty$, moving the basis rightward requires correspondingly more refinement (shown in Fig. 7(e)). However, the p-adaptive method alone cannot compensate for the inability to capture diffusion and advection, resulting in an inaccurate approximation. We have also checked that apart from what is shown in Fig. 7, applying any single scaling,

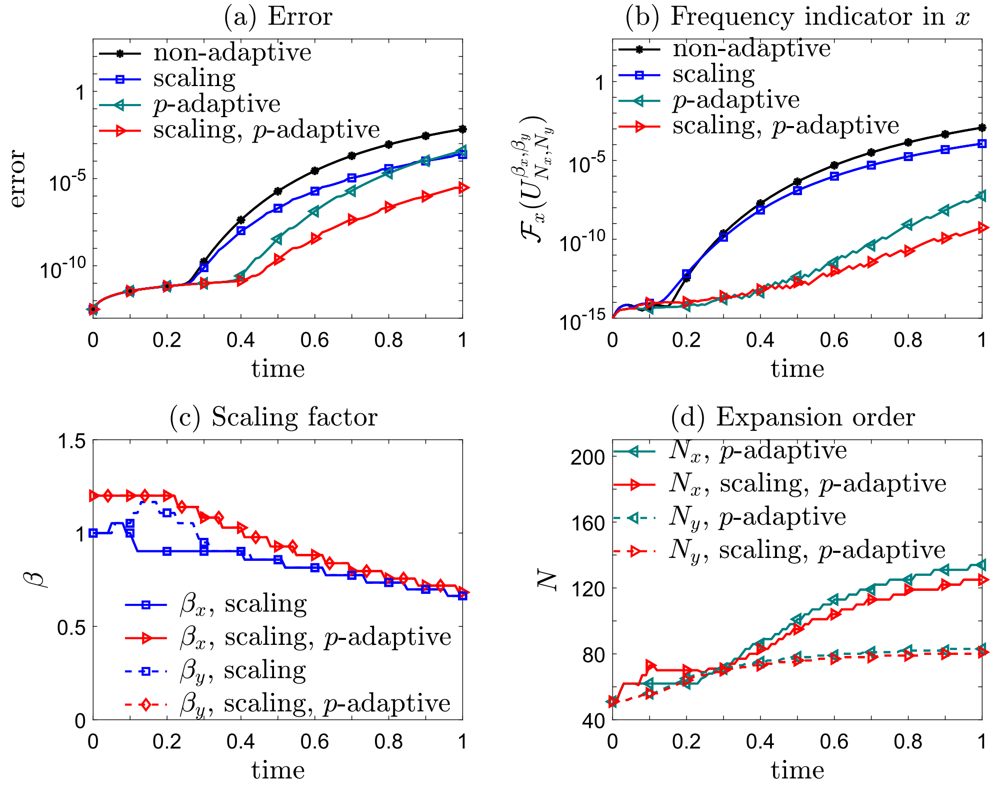

Fig. 8. Numerical solution of the 2-D Schrödinger's equation (4.12). Applying scaling and p-adaptive techniques can capture diffusive and oscillatory behavior of the solution. The solution is heterogeneous in each dimension and requires adjusting the scaling factors and frequency indicators differently in x- and y-directions.

moving or p-adaptive technique, or combining any two of them will all result in a much larger error than employing all three techniques indicated in Fig. 5. The adaptive spectral method produced an error of 3.4572×10^{-8} and required 162.6 seconds of laptop run-time. If we use a fixed $N = 116$, which is the largest expansion order during $t \in [0, 1]$, while activating the scaling and moving techniques 199.2 seconds of run-time is required for an error of 2.0661×10^{-8}. This example verifies that the p-adaptive technique can provide computational savings through adaptive adjustment of the expansion order while maintaining an equivalent accuracy as by using the largest expansion order.

Example 7. We solve the following 2-D Schrödinger's equation in $\mathbb{R}^2 \times \mathbb{R}^+$:

$$i\partial_t \psi(x, y, t) = -\Delta\psi(x, y, t), \tag{4.12}$$

that admits the diffusive and increasingly oscillatory analytic solution

$$\Psi(x, y, t) = \frac{1}{\sqrt{\zeta_x + it}} \exp\left[-\frac{x^2}{4(\zeta_x + it)}\right] \frac{1}{\sqrt{\zeta_y + it}} \exp\left[\frac{y^2}{4(\zeta_y + it)}\right]. \tag{4.13}$$

The function is heterogeneous and requires different scaling and adjustment of the expansion orders in each dimension. We shall still solve the weak form by similar schemes described in Eqs. (4.4) and (4.5) to advance time. Since the function is not advecting over time, we deactivate the moving technique by setting the maximal displacement to be 0. We set $\zeta_x = 0.5, \zeta_y = 0.3$ in Eq. (4.13) giving rise to a function that is more oscillatory and diffusive in x. The initial scaling factors are $\beta_x = 1, \beta_y = 1.2$ and the initial expansion orders were set to $N_x = N_y = 50$, with constraints $N_{x,\min} = N_{y,\min} = 0$, $N_{x,\max} = N_{y,\max} = 6$. We used the scaling parameters $q_x = q_y = \nu_x^{-1} = \nu_y^{-1} = 0.95$ and the p-adaptivity parameters $\eta_x = \eta_y = 1.02, \gamma_x = \gamma_y = 1$.

Because the frequency indicators are applied in both directions, the spectral method with the p-adaptive and scaling techniques leads to the smallest error (Fig. 8(a)). In Fig. 8(b) we plot frequency indicators in the x-direction and show that the spectral method with both scaling and p-adaptive techniques gives rise to the smallest values. Furthermore, since the function is more diffusive and oscillatory in x, β_x, the scaling factor in x is decreased more than β_y when only scaling is used, as shown in Fig. 8(c). Expansion orders N_x in both scaling and scaling + p-adaptive methods increases faster than N_y, as shown in Fig. 8(d). Fig. 8(d) also shows that proper scaling can avoid unnecessary increases in the expansion order, in

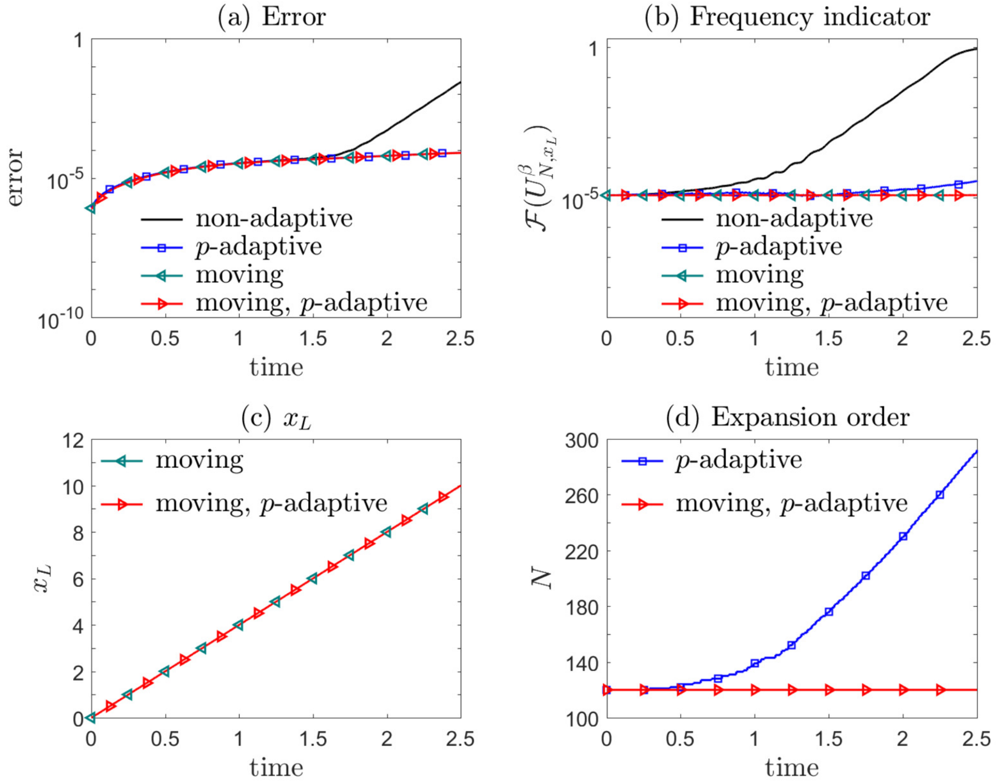

Fig. 9. Numerical solution of the nonlinear Schrödinger's equation (4.14). The solution translates rightward which may cause a false increase in the frequency indicator leading to a large error if the moving technique is not applied. If moving is not applied, the expansion order will need to be increased to give an accurate solution. However, by properly moving the basis functions rightward using the moving technique, accuracy can be maintained without increasing the expansion order. Therefore, the moving technique is required in addition to the p-adaptive method.

this case, N_y. As shown in Fig. 8(a), increasing the expansion order without scaling leads to an even larger error at $t = 1$ than that obtained under pure scaling.

For comparison, we also use the spectral method without the p-adaptive technique and fix the expansion orders $N_x = 124$, $N_y = 80$, the largest values reached under the p-adaptive and scaling techniques. The error 3.1852×10^{-5} is comparable to the error 3.0366×10^{-5} of the adaptive method, but the run-time 7.1705×10^4 seconds (when using fixed $N_x = 124$, $N_y = 80$) is significantly larger than the 4.9508×10^4 seconds necessary for the adaptive method. Therefore, using the p-adaptive technique to adjust the expansion order efficiently can significantly reduce computational costs without sacrificing accuracy.

Example 8. We numerically solve the following nonlinear Schrödinger's equation in $\mathbb{R}$ [24]:

$$i\partial_t \psi = \partial_x^2 \psi + 2|\psi|^2 \psi, \quad \psi(x,0) = 2e^{-2ix}\text{sech}(2x), \tag{4.14}$$

which admits an analytic solution

$$\psi(x,0) = 2e^{-2ix}\text{sech}(2x - 8t). \tag{4.15}$$

Clearly, the function translates rightward, requiring a corresponding translation of the basis functions. In Example 5 we have demonstrated that successfully capturing the diffusive behavior of the numerical solution by the scaling technique can prevent unnecessary increase of the expansion order. Here, we show that successfully capturing the advective behavior of the solution can also help avoid unnecessary increase of the expansion order, reducing computational costs. Since the solution does not exhibit diffusive behavior, we use the algorithm described in Fig. 5 but deactivate the scaling technique.

For the p-adaptive technique, we set $\eta = 1.3$, $\gamma = 1$, $N_{\max} = 20$, and $N_{\min} = 0$ while for the moving technique we set $\mu = 1.00005$, $\delta = 0.0005$, $d_{\max} = 0.01$, the initial expansion order $N = 120$, the scaling factor $\beta = 1.3$, and set the timestep $\Delta t = 0.0005$. An explicit third order Runge Kutta scheme is used to forward time.

Spectral methods including the moving technique can achieve the highest accuracy and maintain the smallest frequency indicator as shown by the green and red curves in Figs. 9(a, b), respectively. Since the oscillatory behavior of the solution does not varying over time and the function translates to the right with speed $4s^{-1}$, the p-adaptive technique will not be activated as long as we properly move the basis functions rightward. Translation can be accurately captured by the moving

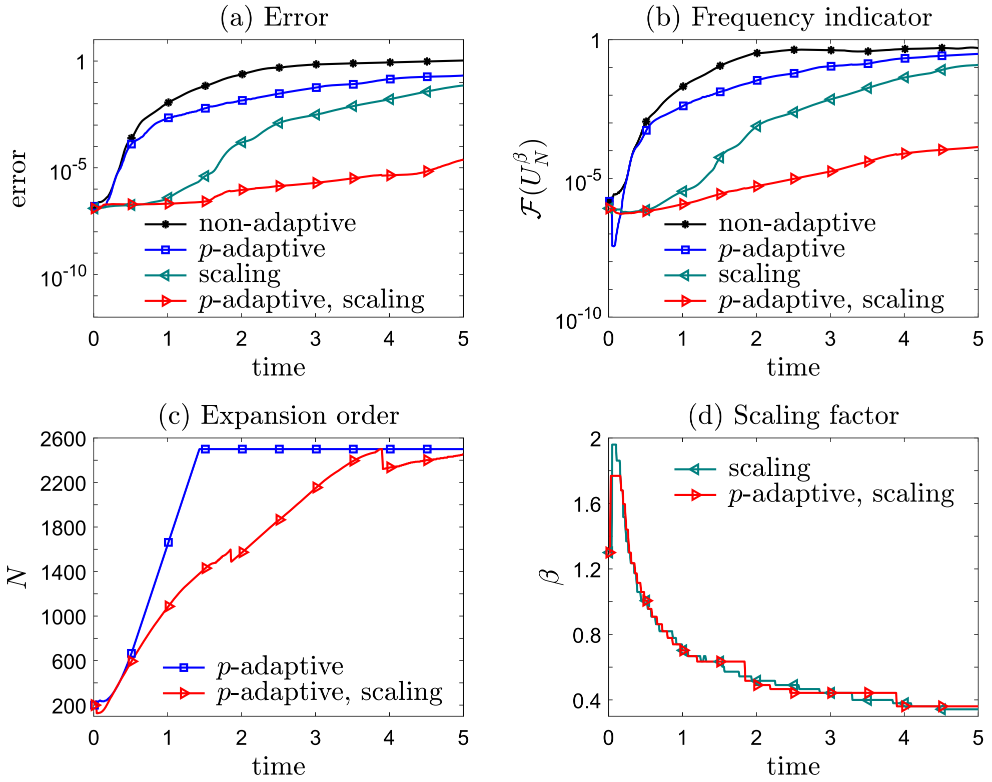

Fig. 10. Numerical solution of Schrödinger's equation with non-vanishing potentials. Rapidly increasing oscillations of the solution over time requires much refinement and proper scaling to maintain accuracy. It is again verified that proper scaling can avoid unnecessary refinement and avoid unnecessary computational burden by adaptively adjusting the scaling factor. Without scaling, the expansion order soon reaches the upper bound for N (the expansion order of the reference solution) and the approximation soon deteriorates due to an inability to further increase N or adjust β and maintain a low frequency indicator. Failure to accommodate the p-adaptive technique will also result in a larger error because of an inability to capture the oscillatory behavior.

technique (Figs. 9(c, d)). However, as shown in Fig. 9(d), without the moving technique, the p-adaptive method increases the expansion order to maintain accuracy, resulting in a higher computational cost. As mentioned in [8], translation will induce a false increase in the frequency indicator. Successfully resolving the translation can be used to prevent unnecessary increases in the expansion order. In this example, the moving and p-adaptive technique requires 2.1569×10^3 seconds of run-time while the p-adaptive technique without moving required 3.8235×10^3 seconds. Thus, it is important to first properly move the basis functions before adjusting the expansion order.

Next, we numerically solve Schrödinger's equation with non-vanishing potentials.

Example 9. We numerically solve the following standard Schrödinger's equation (4.1) equivalent to Example 2 in [14] with the potentials

$$V_{\mathrm{ex}}(x,t) = \frac{50}{\sqrt{\pi}}\sin(10t)\int_{-\infty}^{x}\exp(-z^2)\mathrm{d}z,\ \ V(x) = -10\left[e^{-10(x-1)^2} + e^{-10(x+1)^2}\right]. \tag{4.16}$$

Given an even function as the initial condition for Example 2 in [14], the solution is also an even function and the solution of Eq. (4.1) obeys $|\psi(-x,t)| = |\psi(x,t)|$. No bias towards $-\infty$ or $+\infty$ is preferred. Therefore, we use the Hermite function basis and apply the algorithm described in Fig. 5 but deactivate the moving technique by setting $d_{\max} = 0$. We use the same initial condition as in Example 6 and set $\eta = 1.025, \gamma = 1, q = 0.95, \nu = q^{-1}, N_{\min} = 0, N = 200, \underline{\beta} = 0.3, \overline{\beta} = 2$, and $\beta_0 = 1.3$ at $t = 0$ with the maximum expansion order increment in each step $N_{\max} = 20$.

The reason we set $\gamma = 1$ is that the expansion order N needs to be increased quickly to catch up with the rapidly increasing oscillatory behavior of the numerical solution. We set a uniform timestep $\Delta t = 0.01$ and use only the scaling technique with fixed $N = 2500$ to find the reference solution. For the p-adaptive method, we added an additional restriction that the expansion order of the reference solution cannot exceed $N = 2500$.

We can easily see that the spectral method with both scaling and p-adaptive techniques outperforms the non-adaptive spectral method or with only one of these two techniques employed (shown in Fig. 10(a)). The frequency indicator of

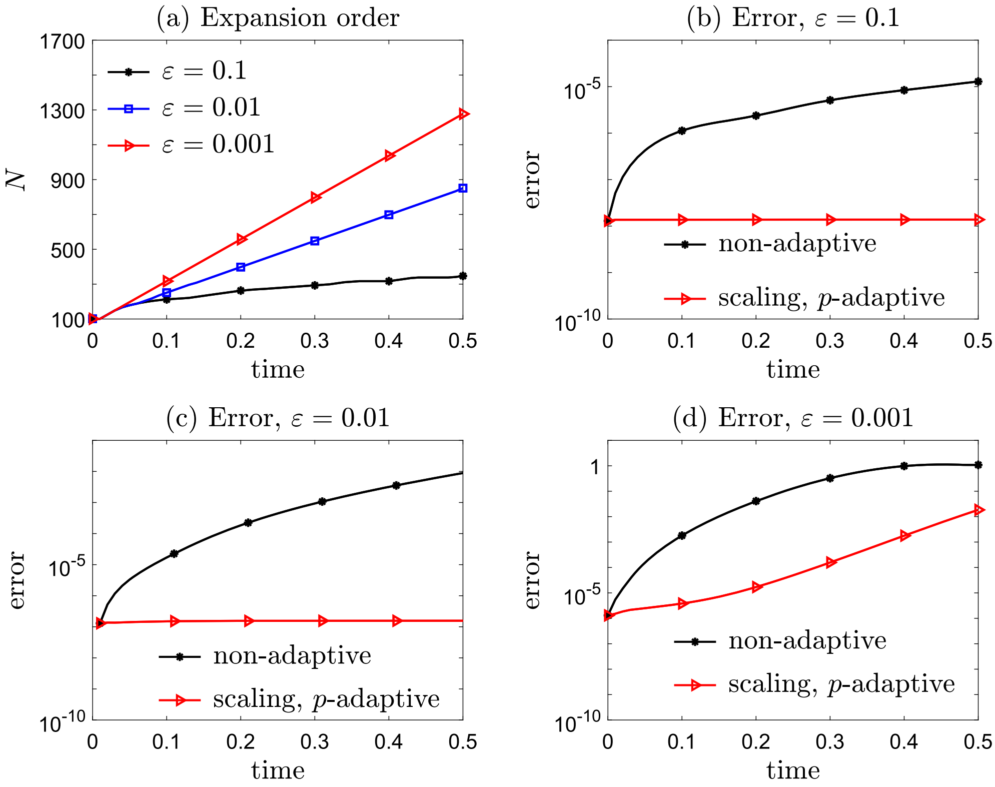

Fig. 11. Numerical solution of Schrödinger's equation (4.17) in the small ε limit using the time-dependent potential given in Eq. (4.18). Rapidly increasing oscillations of the solution require significant refinement by the p-adaptive technique in order to maintain accuracy. The expansion order increases faster over time as ε becomes smaller. In general, the p-adaptive technique is appropriate for solving Eq. (4.17) in the mesoscopic regime for ε that is not too small.

using both scaling and p-adaptive techniques is also the smallest (Fig. 10(b)), and the similarity between the frequency indicator and error is again confirmed as stated in [8]. Moreover, the unscaled method will result in a larger expansion order (Fig. 10(a)), leading to excessive refinement with no improvement in accuracy (Fig. 10(a)). In this example, the coarsening procedure will not lead to a large increase in the frequency indicator and does not significantly compromise accuracy (Figs. 10(b, c)). Finally, the scaling factors of the p-adaptive spectral method and the non-p-adaptive spectral method trend similarly over time; they both decrease after experiencing an initial, transient increase (Fig. 10(d)).

Example 10. Finally, we consider solving Schrödinger's equation,

$$i\partial_t \psi(x,t) = -\varepsilon\partial_x^2 \psi(x,t) + \frac{1}{\varepsilon} V(x,t), \tag{4.17}$$

in the semiclassical regime in which the solution can become more oscillatory over time, especially when $\varepsilon \to 0^+$ as illustrated in [25]. A p-adaptive technique to increase the expansion order is thus needed. We investigate whether our p-adaptive technique can successfully solve Eq. (4.17) as $\varepsilon \to 0^+$ and how the evolution of expansion order N depends on ε.

We assume a time-dependent potential

$$V(x,t) = \sin(t/8)\exp(-10x^2) \tag{4.18}$$

which is even in $\mathbb{R}$ and use the same even initial condition as in Example 6. Since the solution remains even, no translation of the basis functions is needed. Therefore, as in Example 9, we deactivate the moving technique by setting $d_{\max} = 0$. We set $\eta = 1.02, \gamma = 1, q = 0.95, \nu = q^{-1}, N_{\min} = 0, N = 100, \underline{\beta} = 0.3, \overline{\beta} = 2$, and $\beta_0 = 1.3$ at $t = 0$ and impose a maximum expansion order increment $N_{\max} = 24$ at each timestep $\Delta t = 0.01$. As a reference solution, we solve Eq. (4.17) using a fixed $N = 2500$ with the scaling technique and investigate the cases $\varepsilon = 0.1, 0.01$, and 0.001.

Since the solution increases its oscillations faster as ε becomes smaller, the expansion order needs to be increased accordingly. As shown in Fig. 11, under the p-adaptive technique, the smaller the ε, the faster the rate of increase of the expansion order N. In this example, no intrinsic diffusion of the solution is detected and scaling is not activated in the p-adaptive technique as long as the expansion order is properly increased. Figs. 11(b, c, d) show the errors for $\varepsilon = 0.1, 0.01,$

and 0.001, respectively. Without adaptive methods, the errors increase significantly as ε decreases, but by employing p-adaptivity, the expansion order is adjusted to control the errors, dramatically reducing their increase across time, as shown in Figs. 11(b, c).

When ε becomes even smaller, the solution becomes extremely oscillatory and the expansion order needs to be increased too fast even for the current implementation of the p-adaptive method to accommodate (see $\varepsilon = 0.001$ in Fig. 11(d)). Very small ε in Eq. (4.17) poses an intrinsic numerical difficulty that requires extremely large expansion order N. In the extremely small ε regime, methods like Magnus-Zassenhaus splittings [25], which becomes more accurate as $\varepsilon \to 0^+$, could be used. Thus, our p-adaptive technique is most applicable to the mesoscopic regime of a Schrödinger's equation of the form Eq. (4.17) in which ε is not too small. Nonetheless, our p-adaptive technique can efficiently capture oscillations and complements existing methods designed for very small ε.

5. Summary and conclusion

In this paper, we proposed a frequency-dependent p-adaptive technique that adjusts the expansion order for spectral methods. We demonstrated its applicability to time-dependent problems with varying oscillatory behavior. In order to develop efficient numerical methods for problems requiring solutions in unbounded domains, we also combined the p-adaptive technique with scaling (r-adaptivity) and moving (h-adaptivity) methods to devise a complete adaptive spectral method that can successfully deal with diffusion, advection, and oscillation. Through a number of numerical examples, we explored the relationship among the three building blocks: the scaling, moving, and p-adaptive techniques. In particular, the proposed p-adaptive technique enables us to adjust the expansion order dynamically, boosting efficiency of the spectral method. We also investigated the relationship between scaling and p-adaptive techniques for spectral methods in unbounded domains, both of which depend on the same frequency indicator.

Our adaptive spectral method was also used to numerically solve different variations of Schrödinger's equation. The solutions to these examples can contain rapid oscillations across the whole domain that evolve in time, posing numerical difficulties for existing numerical methods that truncate the domain. However, this type of problem can be efficiently resolved by our p-adaptive spectral methods. We find the proposed approaches are most effective in the mesoscopic, semi-classical regime of Schrödinger's equation where ε is not too small.

Further analysis of the proposed methods can be performed. The relationship among the adaptive techniques for spectral methods, scaling, moving, refinement and coarsening, can be further studied and rigorous numerical analysis for these techniques should be investigated. Furthermore, fast algorithms with mapped Chebyshev polynomials for solving PDEs in unbounded domains have been developed using the fast Fourier transform [20]. Thus, generalizing these adaptive methods for mapped Jacobi polynomials may be a compelling future research direction.

Declaration of competing interest

The authors declare that they have no known competing financial interests or personal relationships that could have appeared to influence the work reported in this paper.

Acknowledgements

MX and TC acknowledge support from the National Science Foundation through grant DMS-1814364 and the Army Research Office through grant W911NF-18-1-0345. SS acknowledges financial support from the National Natural Science Foundation of China (No. 11822102) and Beijing Academy of Artificial Intelligence (BAAI). Computational resources were provided by the High-performance Computing Platform at Peking University. The authors are grateful to the handling editor and referees for their valuable suggestions.

References

[1] S. Tsynkov, Numerical solution of problems on unbounded domains. A review, Appl. Numer. Math. 27 (1998) 465–532.
[2] M. Xia, C.D. Greenman, T. Chou, PDE models of adder mechanisms in cellular proliferation, SIAM J. Appl. Math. 80 (2020) 1307–1335.
[3] H. Tang, T. Tang, Adaptive mesh methods for one- and two-dimensional hyperbolic conservation laws, SIAM J. Numer. Anal. 41 (2003) 487–515.
[4] I. Babuska, J.E. Flaherty, W.D. Henshaw, J.E. Hopcroft, J.E. Oliger, T. Tezduyar, Modeling, Mesh Generation, and Adaptive Numerical Methods for Partial Differential Equations, Vol. 75, Springer Science & Business Media, 2012.
[5] W. Ren, X.-P. Wang, An iterative grid redistribution method for singular problems in multiple dimensions, J. Comput. Phys. 159 (2000) 246–273.
[6] R. Li, W. Liu, H. Ma, T. Tang, Adaptive finite element approximation for distributed elliptic optimal control problems, SIAM J. Control Optim. 41 (2002) 1321–1349.
[7] J. Shen, L.L. Wang, Some recent advances on spectral methods for unbounded domains, Commun. Comput. Phys. 5 (2009) 195–241.
[8] M. Xia, S. Shao, T. Chou, Efficient scaling and moving techniques for spectral methods in unbounded domains, arXiv:2009.13170, 2020, SIAM J. Sci. Comput., to appear.
[9] S. Shao, T. Lu, W. Cai, Adaptive conservative cell average spectral element methods for transient Wigner equation in quantum transport, Commun. Comput. Phys. 9 (2011) 711–739.
[10] M. Dumbser, M. Käser, E.F. Toro, An arbitrary high-order discontinuous Galerkin method for elastic waves on unstructured meshes, V: local time stepping and p-adaptivity, Geophys. J. Int. 171 (2007) 695–717.

[11] B.L. Karihaloo, Q. Xiao, Accurate determination of the coefficients of elastic crack tip asymptotic field by a hybrid crack element with p-adaptivity, Eng. Fract. Mech. 68 (2001) 1609–1630.
[12] X. Yang, J. Zhang, Computation of the Schrödinger equation in the semiclassical regime on an unbounded domain, SIAM J. Numer. Anal. 52 (2014) 808–831.
[13] H. Han, J. Jin, X. Wu, A finite-difference method for the one-dimensional time-dependent Schrödinger equation on unbounded domain, Comput. Math. Appl. 50 (2005) 1345–1362.
[14] B. Li, J. Zhang, C. Zheng, Stability and error analysis for a second-order fast approximation of the one-dimensional Schrödinger equation under absorbing boundary conditions, SIAM J. Sci. Comput. 40 (2018) A4083–A4104.
[15] X. Antoine, A. Arnold, C. Besse, M. Ehrhardt, A. Schädle, A review of transparent and artificial boundary conditions techniques for linear and nonlinear Schrödinger equations, Commun. Comput. Phys. 4 (2008) 729–796.
[16] T.Y. Hou, R. Li, Computing nearly singular solutions using pseudo-spectral methods, J. Comput. Phys. 226 (2007) 379–397.
[17] S.A. Orszag, On the elimination of aliasing in finite-difference schemes by filtering high-wavenumber components, J. Atmos. Sci. 28 (1971) 1074.
[18] J. Shen, T. Tang, L.L. Wang, Spectral Methods: Algorithms, Analysis and Applications, Springer Science & Business Media, New York, 2011.
[19] C. Moler, C. Van Loan, Nineteen dubious ways to compute the exponential of a matrix, twenty-five years later, SIAM Rev. 20 (1978) 801–836.
[20] C. Sheng, J. Shen, T. Tang, L.-L. Wang, H. Yuan, Fast Fourier-like mapped Chebyshev spectral-Galerkin methods for PDEs with integral fractional Laplacian in unbounded domains, SIAM J. Numer. Anal. 58 (2020) 2435–2464.
[21] C. Canuto, R.H. Nochetto, R. Stevenson, M. Verani, On p-robust saturation for hp-AFEM, Comput. Math. Appl. 73 (2017) 2004–2022.
[22] P. Antonietti, C. Canuto, M. Verani, An adaptive hp–DG–FE method for elliptic problems: convergence and optimality in the 1D Case, Commun. Appl. Math. Comput. 1 (2019) 309–331.
[23] B.-Y. Guo, L.-L. Wang, Jacobi interpolation approximations and their applications to singular differential equations, Adv. Comput. Math. 14 (2001) 227–276.
[24] T.R. Taha, M.J. Ablowitz, Analytical and numerical aspects of certain nonlinear evolution equations. II. Numerical, nonlinear Schrödinger equation, J. Comput. Phys. 55 (1984) 203–230.
[25] A. Iserles, K. Kropielnicka, P. Singh, Solving Schrödinger equation in semiclassical regime with highly oscillatory time-dependent potentials, J. Comput. Phys. 376 (2019) 564–584.